MATERIALS CHEMISTRY
FRONTIERS

REVIEW

View Article Online
View Journal | View Issue



Cite this: *Mater. Chem. Front.*, 2023, **7**, 2120

# Recent developments in transition metal-based MOFs for electrocatalytic water splitting emphasizing fundamental and structural aspects

Ragunath Madhu, [ab] Arun Karmakar, [ab] Krishnendu Bera, [ab] Sreenivasan Nagappan, [ab] Hariharan N Dhandapani, [ab] Aditi De, [ab] Suprobhat Singha Roy [ab] and Subrata Kundu *[ab]

Received 24th January 2023,
Accepted 18th February 2023

DOI: 10.1039/d3qm00089c

rsc.li/frontiers-materials



Energy scarcity and environmental pollution are major threats to the long-term viability of modern civilization. Electrocatalytic water splitting is a crucial technology for environmentally friendly and long-lasting energy storage and a clean way to make hydrogen. Metal–organic frameworks have become the most capable multifunctional materials in recent years because of their enormous surface areas, tunable permeability, simplicity in compositional alteration, and capacity to be used as predecessors for a variety of morphological shapes. In this review, MOFs and their derivatives as an electrocatalyst for the OER are well defined. An overview of the fundamental ideas and important evaluation criteria related to the electrochemical water-splitting reaction is provided at the outset of this review. Herein, how MOF-based materials will serve as a potential candidate with suitable synthetic methods in the near future with respect to detailed fundamental and electronic structural outcomes has been summarized. Additionally, this review describes the difficulties and opportunities of the MOF-based electrocatalysts for the water splitting process. Finally, this review will pave an effective pathway for constructing a sustainable MOF production, which will help the reader in producing sustainable and greener hydrogen technology.

[a] *Academy of Scientific and Innovative Research (AcSIR), Ghaziabad-201002, India*
[b] *Electrochemical Process Engineering (EPE) Division, CSIR-Central Electrochemical Research Institute (CECRI), Karaikudi-630003, Tamil Nadu, India. E-mail: skundu@cecri.res.in, kundu.subrata@gmail.com; Fax: (+91) 4565-241487; Tel: (+91) 4565-241487*

**Ragunath Madhu**

*Ragunath Madhu received his BSc degree (2014–2017) from 'The Gandhigram Rural Institute' Dindigul, India and his MSc degree from University of Madras, Chennai, India, in analytical chemistry (2017–2019). As he was top of the university in his MSc, he received a gold medal and was awarded an INSPIRE scholarship (SRF) in March 2020 by DST, New Delhi. Ragunath Madhu joined Dr Subrata Kundu's research group in August 2020 and his PhD thesis work is mainly focused on catalysis, SERS, and electrocatalytic water splitting applications.*

**Arun Karmakar**

*Arun Karmakar received his Bachelor of Science degree from Derozio Memorial College under West Bengal State University (2017) and received his Master of Science degree from the same university (2019) with specialization in inorganic chemistry. While pursuing his MSc, he qualified for the NET (National Level Eligibility Test) and an SRF (Junior Research Fellowship) from CSIR, New Delhi, with an all-India ranking of "23" (December 2018, chemical science). Arun Karmakar joined Dr Subrata Kundu's lab in August 2019 and is working on his PhD thesis, mainly focusing on "the synthesis of nano-structured materials for catalysis, electrocatalysis, and SERS applications".*

 

## Introduction

The creation of clean, sustainable alternative energy to fossil fuels is necessary to address global warming and the climate problem. Hydrogen is regarded as a clean fuel due to its high energy density (142 kJ $mol^{-1}$) and having zero impacts on the environment.[1,2] Despite this encouraging outlook, a green, sustainable, and effective technology for producing hydrogen on a big scale is still sorely needed. The current commercial techniques of producing hydrogen (such as steam reforming) depend on the use of hydrocarbons and further release an enormous amount of greenhouse gases like $CO_2$. As an alternative, electrochemical water splitting is a viable technology that can generate vast amounts of high purity hydrogen under benign conditions with an only byproduct of water. The hydrogen evolution reaction (HER) and the oxygen evolution reaction (OER) are the two half-reactions involved in electrochemical water splitting.[3–5] Theoretically, the nominal breakdown voltage for the splitting of water is 1.23 V, but in practical electrolytic investigations, an overpotential ($\eta$) is needed to go beyond the kinetic barrier and produce hydrogen at a high adequate rate. Overpotential increases energy consumption, which lowers the efficiency of electrochemical water splitting and the ability to compete in terms of economy. Electrocatalysts can increase the current density at a given voltage by

**Krishnendu Bera**

*Krishnendu Bera received his BSc degree from Ramakrishna Mission Vivekananda Centenary College (Rahara, West Bengal) affiliated with West Bengal State University (2018) and obtained his MSc degree from the same university (2020) with specialization in 'Physical Chemistry'. While pursuing his MSc, he qualified for the NET (National Level Eligibility Test) as a JRF (Junior Research fellowship) from CSIR, New Delhi. In addition, he qualified for the GATE (Graduate Aptitude Test in Engineering) in 2020. Now, he has been pursuing his PhD under Dr Subrata Kundu in CSIR-CECRI from January 2021 and his PhD thesis will be mainly focused on ''Development of non-precious transition metal-based electrocatalysts for water splitting applications''.*

**Sreenivasan Nagappan**

*Sreenivasan Nagappan received his Bachelor of Science degree from Gobi Arts and Science College under Bharathiar University (2015-2018) and received his Master of Science degree from University of Madras (2018-2020) with specialization in Inorganic Chemistry. As he was top of the university in his MSc, he received a gold medal and was awarded an INSPIRE scholarship (JRF) in March 2021 by DST, New Delhi. Currently, he has been pursuing his PhD under Dr Subrata Kundu since August 2021 in the field of ''Electrospun Transition Metal based Modified Nanofibers for Water Electrolysis''.*

**Hariharan N Dhandapani**

*Hariharan N Dhandapani pursued his Bachelor of Science degree from Sacred Heart college under Thiruvalluvar University (2012) and pursued his Master of Science degree from the Madurai Kamaraj University (2014) in General Chemistry. Afterwards, he qualified for the NET (National Level Eligibility Test) and a JRF (Junior Research fellowship) from CSIR, New Delhi, with an all India ranking of ''87'' (November 2020, chemical science). Hariharan N Dhandapani join under Dr Subrata Kundu in August 2021 and is working on his PhD thesis mainly focused on ''modified transition metal double layer hydroxides for water splitting applications''.*

**Aditi De**

*Aditi De received her Bachelor of Science degree from Bankura Christian College under The University of Burdwan (2017) and received her Master of Science degree from the West Bengal State University (2019) with a specialization in organic chemistry. She qualified for the WB-SET (West Bengal State Level Eligibility Test), and the NET (National Level Eligibility Test) for eligibility for Assistant Professor in Chemical Science. She also passed the GATE (Gratitude Aptitude Test in Engineering) exam and joined Dr Subrata Kundu's research group in April 2022. She is currently working towards her PhD thesis, mainly focusing on electrocatalytic water splitting applications.*

minimizing the overpotential and catalyzing electrochemical processes. Therefore, an effective electrocatalyst with high catalytic performance and high static stability is mandatory for large-scale viable hydrogen generation through the electrochemical method. Presently, electrocatalysts composed of noble metals are considered as state of the art for the OER (Ir or Ru-based catalysts) and HER (Pt-based catalysts).[6–8] Apparently, due to their high price and limited availability, these materials are restricted for commercial applications. Thus, the development of low-cost non-noble metal-based electrocatalysts for water splitting will be a crucial factor for the commercialization of water electrolysis. Over the past several years, there has been significant progress in the creation of such electrocatalysts from earth-abundant metals.[9,10] Electrocatalysts often exhibit different kinetics for the HER and OER, and their performance is greatly influenced by the pH environment. Presently, the electrocatalysts which show higher performance towards the OER in an alkaline environment will exhibit a poor performance towards the HER in the same environment, whereas in the case of an acidic environment it would be *vice versa*. As a result, high-performance bifunctional electrocatalysts that can simultaneously catalyze both the HER and OER under the same environment are highly crucial and challenging, yet they are currently lacking in efficiency. These bifunctional electrocatalysts can significantly reduce the costs by dramatically facilitating hydrogen generation.[11] Finding highly active electrocatalysts for the water splitting reaction requires significant specific surface area, tunable porosity and more charge transfer capability. These elements are crucial for increasing electron transfer and boosting the mass transit of reactants. Metal organic frameworks (MOFs) are a class of nano-porous crystalline organic framework self-assembled through the coordination of metal ions and an organic linker. Owing to the cage-like structure, MOFs can be employed as a potential candidate for numerous applications like catalysis, sensing, luminescence, drug delivery and imaging, adsorption and separation, and gas and energy storage.[12–16] The main pros of MOFs are their tunable pore size, tunable morphology, high specific surface area, and flexible and tunable chemical functionalities with different organic linkers.[17,18] Besides, the poor conductivity, low stability and micro-regime crystal size of MOFs limit them from many viable electrocatalytic application. Nonetheless, these flaws can be overcome by partial substitution of another active metal ion into the organic network, metal node engineering, creating defects/vacancies and designing derivatives from the MOFs to tune the electronic and structural properties, towards the enhancement of electrocatalytic activity.[19] Also, the first scientific concept of a MOF was put forth in 1995 by the Yaghi research group. MOF-5 is regarded as the most well-liked framework and is said to be the first MOF structure to introduce the idea of reticular chemistry.[20] This has inspired individuals to synthesize and engineer many unique MOF materials using a variety of organic and inorganic SBUs (secondary building units) like zeolite-imidazole framework (ZIF-*n*), iso-reticular metal–organic framework (IRMOF-*n*), Materials of Institute Lavoisier (MIL-*n*), University of Oslo (UiO-*n*), and other series of MOFs. Scheme 1 shows a depiction of the conceptual designing of MOFs using various metal nodes and several organic linkers.[21]

Nevertheless, a thorough analysis specifically focusing on electrocatalytic water splitting is limited, despite the fact that several reviews of MOF-based energy conversion materials have been published providing a general overview of their variety, synthetic techniques, structure, characteristics, and prospective applications. Therefore, a timely review of the relevant studies over the last few years is urgently needed. In this review, we would like to give a brief overview of the most recent developments in MOF-based electrocatalysts in terms of their design and fabrication, characterization, and catalytic

**Suprobhat Singha Roy**

*Suprobhat Singha Roy received his BSc degree (2016-2019) from Ramakrishna Mission Vivekananda Centenary College under West Bengal State University and MSc degree (2019-2021) from School of Chemistry, University of Hyderabad. He has Qualified joint CSIR-UGC NET examination in 2022 and has been awarded with UGC-Junior Research Fellowship. He joined Dr Subrata Kundu's research group in August 2022 and his work mainly focuses on nanomaterial-based catalyst development for electrocatalytic water splitting applications.*

**Subrata Kundu**

*Dr Subrata Kundu received his PhD from the Indian Institute of Technology (IIT), Kharagpur, India in early 2005. Then he moved to University of Nebraska, Lincoln, USA and later to Texas A&M University, College station, Texas, USA as a post-doc fellow (from 2005 to 2010). He is currently working as a Principal Scientist at CSIR-CECRI, Karaikudi, India. Dr Kundu has served as an associate editor of the prestigious 'Journal of Materials Chemistry A' and 'Materials Advances' from the RSC publishers since 2022 and 'Scientific Reports' from 'Nature group publishers' since 2015. Dr Kundu and his co-workers are working in the forefront area of Material Sciences with emphasis on energy, environment, catalysis and electrocatalysis applications.*

 

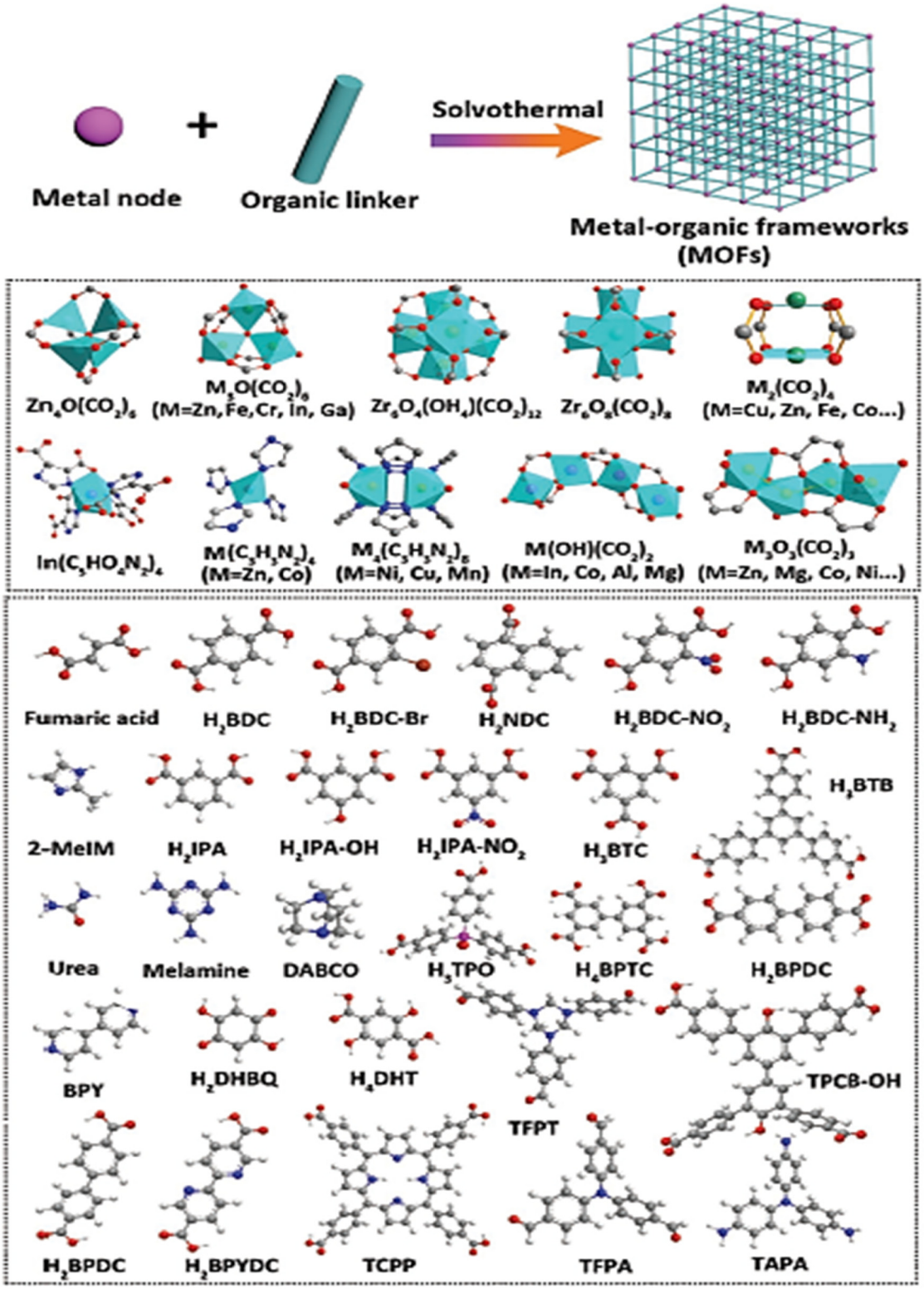


Scheme 1 Schematic depiction of the theoretical designs of different MOFs using various metal nodes and organic linkers. Reprinted with permission from ref. 21. Copyright (2021) Wiley-VCH.

mechanism towards water splitting reactions. In summary, the difficulties and possibilities of using MOF-based materials for water splitting are highlighted. We are confident that reading this review will not only help readers to better comprehend the connections between structure, composition, and efficiency, but also provide fundamental guidelines for methodically

constructing molecular electrocatalysts for energy storage and conversion.

## General oxygen evolution reaction (OER) mechanism

Generally, water splitting is an uphill process in terms of thermodynamics. The two main half-cell reactions of water splitting are the OER at the anode and the HER at the cathode. Whatever the circumstances, the variation in the free energy change ($\Delta G$) of the water splitting reaction at 25 °C and 1 atm equals 237.2 kJ $mol^{-1}$, which equates to the theoretically determined cell voltage of 1.23 V *vs.* RHE required for water splitting. However, both the reactions require a higher voltage than the theoretical voltage to overcome the energy barrier to meet a benchmarking current density. As compared to the HER, the OER is a complex four-electron proton transfer process and depending on the pH of the electrolytes, the reaction pathways of producing $O_2$ usually vary. In alkaline electrolytes, hydroxyl groups ($OH^-$) are oxidized and converted to $H_2O$ and $O_2$ molecules. In acidic media, two water molecules ($H_2O$) are oxidized generating four protons ($H^+$) and one $O_2$ molecule. The OER can be catalyzed more readily in an acidic medium than in an alkaline one by noble and semi-noble metal-based catalysts (such as Ir, Ru, and their oxides). In contrast, electrocatalysts made of active transition metals, are more able to catalyze the OER in alkaline media. The generally accepted reaction pathway is that the oxygen–ligand metal (M) site of the electrocatalyst adsorbs $H_2O$ or $OH^-$ through a single-electron oxidation process, and produces an adsorbed *OH. The *OH is subsequently oxidized to *O, and an intermediate *OOH is created by adsorbing a second $H_2O$ molecule or $OH^-$ ion. The formation of *OOH step is thermodynamically unfavorable because of very weak interaction between –OOH ions and the metal surface (M), which results in a positive free energy for the creation of *OOH species. In order to catalyze the OER by applying lower overpotential, one or more metals in the catalyst must be oxidized to the appropriate higher oxidation counterparts. Finally, the breakdown of the metal oxygen (M–O) bond is the crucial step for the OER and allows the initially pristine M site to be reclaimed. As a result, for a high performance OER process, the M–O bond should be moderate; *i.e.*, it should be neither too strong nor too weak (According to Sabatier's Principle). The following is a step-by-step illustration of the OER process in alkaline and acidic environments.[4,10,14]

In an alkaline environment,

$$M + OH^- \rightarrow M\text{–}OH + e^- \quad (1)$$

$$M\text{–}OH + OH^- \rightarrow M\text{–}O + H_2O + e^- \quad (2)$$

$$M\text{–}O + OH^- \rightarrow M\text{–}OOH + e^- \quad (3)$$

$$M\text{–}OOH + OH^- \rightarrow M + O_2 + H_2O + e^- \quad (4)$$

In an acidic environment,

$$H_2O + M \rightarrow M\text{–}OH + H^+ + e^- \quad (5)$$

$$M\text{–}OH \rightarrow M\text{–}O + H^+ + e^- \quad (6)$$

$$M\text{–}O + H_2O \rightarrow M\text{–}OOH + H^+ + e^- \quad (7)$$

$$M\text{–}OOH \rightarrow M + O_2 + H^+ + e^- \quad (8)$$

where OOH*, O* and OH* represent the intermediates over the surface of the electrocatalyst.

## Parameters involved in and influencing the electrocatalytic kinetics of the OER and HER

Prior to discussing recent developments in the study of MOFs and their derivatives as electrocatalysts, we will first explain the measurement standards for the OER and HER process, which may give an in-depth elucidation of the OER/HER process and a uniform determination technique. As a result, it is important to shed light on a few evaluation parameters, such as overpotential, Tafel slope, turnover frequency (TOF), specific and mass activity, stability and faradaic efficiency (FE).[4,22]

## Overpotential ($\eta$)

Overpotential is one of the vital parameters for evaluating the OER/HER performance of the specified electrocatalyst under certain conditions. The overpotential needed to achieve an operational current density of 10 mA $cm^{-2}$ is a common metric derived from the 12.3% efficiency for the HER and OER in photo-electrochemical water splitting. An electrocatalyst that typically has better activity/performance should result in a lower overpotential at particular current density. The thermodynamic potentials of the HER and OER processes are 0 and 1.23 V *vs.* RHE, respectively.

When compared to their ideal equilibrium value, the system in the HER and OER usually requires extra potential to overcome the kinetic barriers and resistances in real reactions. The extra potential required between the theoretical and experimental potential is known as the overpotential ($\eta$).[22,23]

$$E = E_0 + \frac{RT}{nF}\ln\frac{C_0}{C_R} \quad (9)$$

where $E$ is the applied potential, $E_0$ is the standard potential, $R$ is the ideal gas constant (8.314 510 J $mol^{-1}$ $K^{-1}$), $T$ is the reaction temperature in Kelvin, $F$ is the Faraday constant (96 485.3 C $mol^{-1}$), $n$ is the number of electrons transferred during the reaction (for OER, $n$ is 4 and for HER, $n$ is 2), $F$ is the Faraday constant, and $C_0$ and $C_R$ are the concentrations of oxidized and reduced products, respectively. Also, the pH dependent applied potential can be determined from the equation,

$$E_{eq(RHE)} = E_{eq} + 0.059\ pH \quad (10)$$

By converting the reversible hydrogen potential (RHE) into cell potential, the equation can be expressed as

$$E_{eq(RHE)} = E_{appl} + E_0 + 0.059\ pH \quad (11)$$

 

where $E_{RHE}$ is the converted cell potential, $E_{appl}$ is the applied potential, and $E_0$ is the standard potential. But no reaction will happen at this potential because of the transit restrictions, uncompensated resistance, and activation overpotential/kinetic hurdles. Many different procedures have been used to modify the potentials. So, it is necessary to generate appropriate electrocatalysts, since the kinetic barriers are strongly related to the intrinsic active site of materials and might be defined as charge transfer resistance ($R_{ct}$). The $R_{ct}$ can be expressed as follows:

$$R_{ct} = \frac{RT}{Fi_0} \text{ (At low overpotential)} \quad (12)$$

where $R$ is the ideal gas constant (8.314 510 J $mol^{-1}$ $K^{-1}$), $T$ is the reaction temperature, $F$ is the Faraday constant (96 485 C $mol^{-1}$), and $i_0$ is the exchange current density. Besides, in the case of higher overpotential, $R_{ct}$ mainly depends on the concentration of the electrolyte solution and active surface sites of the electrodes. Upon stirring of the electrolyte solution, the $R_{ct}$ value will decrease during the LSV (linear sweep voltammetry) measurement. Another factor, solution resistance ($R_s$), is mainly related to the geometry of the electrode, the electrolyte concentration and the distance between the reference and counter electrode. This $R_s$ can be corrected as a function of *iR* compensation or subtracted from the obtained current density × solution or uncompensated resistance ($R_{s/u}$) obtained from the Nyquist plot. The equation can be expressed as follows:

$$E_{comp} = E_{meas} - iR_{s/u} \quad (13)$$

where $E_{comp}$ is the $iR_{s/u}$-corrected potential, $E_{meas}$ is the measured potential, $i$ is the measured current density, and $R_{s/u}$ is the solution or uncompensated resistance stemming from EIS (electrochemical impedance spectroscopy).

## Tafel slope ($\beta$)

One of the key studies in the assessment of electrocatalysts for water electrolysis is the Tafel analysis. Tafel analysis of the OER and HER processes is carried out to learn more about the electrocatalyst's inherent kinetics. In actual use, increasing the current density typically needs a disproportionately high overpotential. As a whole, the goal is to create a current density that grows quicker by demanding a smaller overpotential. The relation that correlates current density and overpotential at the electrode–electrolyte interface is expressed as the Butler–Volmer equation, as given below,

$$I = I_0\left[\exp\left(a_A\frac{nF}{RT}\times Z\right) - \exp\left(a_c\frac{nF}{RT}\times Z\right)\right] \quad (14)$$

where $I$ is the current density, $I_0$ is the exchange current density (current at equilibrium potential), and $a_A$ and $a_C$ are the charge transfer coefficients for the anodic and cathodic reactions, respectively; $n$ is the number of electrons transferred, $F$ is the Faraday constant (96 485 C), $R$ is the ideal gas constant, $T$ is the absolute temperature in K and $\eta$ is the overpotential. Upon simplification of the above equation, it is expressed as

$$\eta = a + b\log(i) \quad (15)$$

where $a = 2.303RT\log i_0/aF$, $b = 2.303RT/aF$. From this expression, it is evident that current ($i$) is inversely and overpotential ($\eta$) is directly proportional to $\beta$.[9,22,23] As a result of this inverse correlation, the rate of electron transfer will be higher with lower Tafel slope values with higher a charge transfer coefficient value at the electrode–electrolyte interface. Additionally, the regularity of the extraction approach plays a crucial role. To date, the Tafel plot can be obtained from LSV, EIS procedures and static potentials from chrono-methods. The static potential and steady state current of the EIS and chrono methods, respectively, are the most consistent procedures for Tafel slope determination.

## Turnover over frequency (TOF)

Another crucial factor that has been utilized to assess an electrocatalyst's intrinsic activity at a specific overpotential is turnover frequency. The amount of oxygen/hydrogen that is evolved per unit of time is known as the TOF. The TOF of the catalyst can be determined by the below expression:

$$TOF = \frac{JN_A}{nF\tau} \quad (16)$$

where $j$ stands for the current, $N_A$ for the Avogadro constant, $n$ for the number of electrons transferred, and $\tau$ for the surface or overall concentration of the catalyst in terms of atoms. The obtained TOF values, which are based on the oxidation/reduction of a redox pair, can be used to justify the intrinsic activity of a catalyst and will not change at greater mass loadings. The observed current density will vary depending on the catalyst's mass loading. So, it is essential to determine the TOF value of a catalyst to determine the actual activity of a catalyst. Therefore, first the surface area must be determined from the oxidation/reduction peak in order to evaluate the observed OER/HER activities. As such, TOF can be calculated from the regions that are oxidized or reduced during the $O_2/H_2$ evolution.[2,4,22]

## Specific and mass activity

Another essential parameter that primarily deals with the exposure of active sites of the electrode surface is the roughness factor or electrochemical active surface area (*i.e.*, specific activity) of an electrocatalyst. Before discussing electrochemically active surface area (ESCA), it is necessary to understand that OER catalysts can function as capacitors at the film–electrolyte interface. Therefore, a legitimate technique to determine the electrochemically active surface area is by calculating the double-layer capacitances ($C_{dl}$) of the electrocatalyst in a non-faradaic region to eliminate the faradaic current. Since the ECSA is proportionally related to the $C_{dl}$ value,[24] by employing the expression given below the ECSA can be calculated for an

electrocatalyst:

$$\mathrm{ECSA} = \frac{C_{\mathrm{dl}}}{C_{\mathrm{s}}} \quad (17)$$

where $C_s$ is the flat electrode surface. The number of ions that accumulate on a catalyst surface mainly depends on the exposed area and the applied scan rate for various electrode materials. Additionally, when it comes to materials developed on conducting substrates like 3D foams the surface area will be enormous, which simultaneously increases the activity also. Upon developing materials over 3D foam, the mass of the catalyst loading might be higher. Therefore the ECSA normalized current densities will allow for a more accurate insightful assessment of a catalyst's activity.[4] Another quantitative active parameter used to determine the intrinsic activity of an electrocatalyst is mass activity, which is nothing, but the current is normalized with the catalyst loading. It is expressed in ampere per gram (A $g^{-1}$) or milliampere per milligram (mA $mg^{-1}$).[2]

## Stability

The long-term/static stability is another important criterion for measuring the quality of electrocatalysts in addition to their exceptional activity and selectivity. In the case of the OER and HER, high scan rate CV cycling studies are typically used to verify a catalyst's stability across hundreds or even thousands of cycles and also by the chronoamperometric or chronopotentiometric investigations. In the former one, the difference in overpotential before and after CV cycles (>1000 cycles) at benchmarking current density (10 mA $cm^{-2}$) shows that the deterioration is small, so the catalyst is thought to be stable. Now, let's talk about a catalyst's stability studies while exposed to a constant potential [chronoamperometry (CA)] or constant current density [chronopotentiometry (CP)]. It is evaluated that a catalyst is stable when the CA/CP curve exhibits minimal variations for more than 12 hours (according to reports) at a steady current density or potential. In conclusion, the catalyst showing negligible degradation in the current density after 12 hours of chrono studies or a negligible difference in the overpotential after 12 hours will be recognized as parameters in evaluating the stability of a catalyst for longer-term operation.[2,25]

## Faradaic efficiency (FE)

Another quantitative criterion that is applied to both the HER and OER is faradaic efficiency. It can be described as an electrocatalyst's efficiency, in transferring electrons from an external circuit over an interface to an electroactive species to cause a reaction. The detection of faradaic efficiency by electrochemical RRDE (rotating ring disc electrode) is a reliable method, but limited only for the OER. The catalytic active material is drop cast on an RRDE disc (glassy carbon (GC)) without masking or affecting the Pt ring. Following that, the same potential window of the OER has to apply for the GC disc by constantly maintaining the oxygen reduction reaction (ORR) towards the Pt ring. The potential of the ORR is different for different electrolytes. The FE of an OER catalyst can be calculated from the below equation;

$$\mathrm{FE} = \frac{I_{\mathrm{R}} n_{\mathrm{D}}}{I_{\mathrm{D}} n_{\mathrm{R}} N_{\mathrm{CL}}} \quad (18)$$

where $I_R$ and $I_D$ stands for the current at the ring and disc, respectively, $n_R$ and $n_D$ are the numbers of electrons transferred at the ring and disc, respectively, and $N_{CL}$ is the collection efficiency of the RRDE. Another method of determining the FE is the integration of the amount of $O_2/H_2$ evolved from the chronoamperometric or chronopotentiometric analysis. The obtained results are compared with the conventional water gas displacement method or the gas chromatography technique. Hence, the FE of the catalyst being studied is calculated as the ratio of the amount of gas determined by the theoretical technique and a practical method. Among the above-mentioned parameters, the overpotential, Tafel slope, TOF and stability parameters are obligatory to examine the activity of an electrocatalyst.[2,26]

## Synthetic methods of MOFs

Scheme 2 illustrates the synthetic methods involved in and that influence the synthesis of MOF-based materials. The variables that mainly influence the MOF synthesis are time, temperature, nature of solvent, type of metal and organic linkers used, and the existence of oppositely charged ions and reaction kinetics which are responsible for the nucleation and growth of crystals. Most often, the liquid phase is used to synthesize MOFs by combining solutions of the ligand and the metal salt. The solvent is selected based on its level of reactivity, redox potential, and solubility. Because the solvent plays a major role in bringing the kinetics and thermodynamics of the reaction.

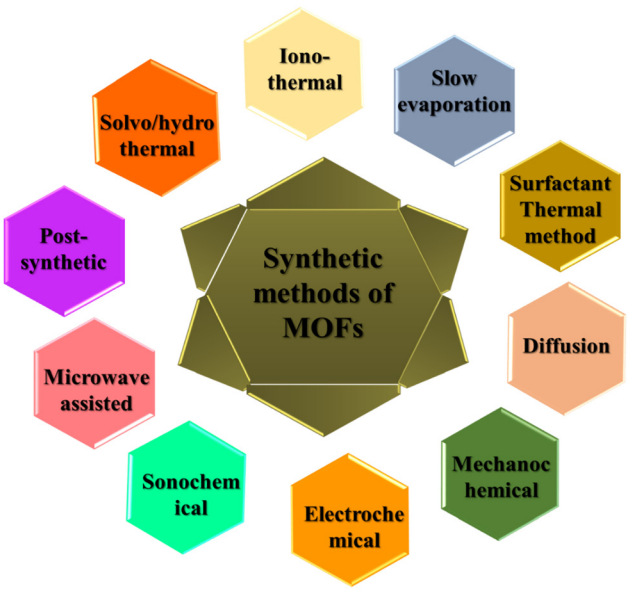


Scheme 2 Methods available for the synthesis of MOF materials.

 

Apart from liquid phase synthesis, solid phase synthesis is easier and faster, but obtaining single crystals and its structure is limited compared to liquid phase synthesis. Another method is called a slow evaporation method, from which a perfect crystal structure of MOFs was obtained. Besides, solvothermal, iono-thermal, diffusion, mechanochemical, electrochemical, sonochemical, template, surfactant-thermal, microwave-assisted, micro-emulsion and post-synthetic methods have been employed as alternatives for the synthesis of MOFs.

## Solvo/hydro-thermal method

Synthesizing MOFs through the solvo/hydrothermal method is considered as a 'prestigious' method. These reactions typically take place in closed vessels at autogenous pressure above the solvent's boiling point at high temperatures between 50–260 °C, for longer time. In some cases, like kinetically inert ions, the temperature is hiked to promote bond formation and assure appropriate crystallization. Moreover, the surface morphology of the crystals is largely influenced by temperature, and even prolonged reaction durations might result in the breakdown of the finished product. Crystal growth is impacted by the cooling rate, which must be extremely slow. During solvothermal reaction, high-boiling organic solvents like dimethyl formamide (DMF), diethyl formamide (DEF), acetonitrile, acetone, ethanol, methanol, or mixtures of solvents can also be used to avoid solubility issues. At the time of reaction, new ligands may be generated inside the reaction vessel as a result of the starting material, which undergoes unexpected chemical changes that are not possible under milder synthetic conditions. This process is less expensive, quicker, and produces cleaner results.[27]

## Iono-thermal method

The iono-thermal method is a sub-class of solvo/hydrothermal method and the name 'iono' denotes ionic liquids. Here, ionic liquids are used as solvents and templates for some reactions. Due to their low vapor pressure, high solubility for organic molecules, high thermal stability, and non-flammability, ionic liquids are more eco-friendly reagents than traditional organic solvents. These advantages make them suitable reagents for the synthesis of other kinds of materials like zeolites and chalcogenides, as well as MOFs. Ionic liquids have received a lot of attention recently as potential alternatives for the synthesis of MOFs since they provide both cations and anions as counter ions and also act as templates for some of the MOF frameworks.[27,28]

## Surfactant-thermal method

Surfactants are typically organic substances that have both hydrophilic and hydrophobic groups. While hydrophobic groups often tend to be oil-soluble yet hydrophobic, polar hydrophilic groups are water-soluble and oil-insoluble. The amphiphilic property of surfactants allows them to self-assemble into a variety of micelles in aqueous and organic solutions. These micelles can be used as templates or structure-directing agents to regulate the sizes and shapes of the catalyst material. In reality, surfactants have a variety of unique solvent properties, such as low vapour pressure, and excellent thermal stability. Surfactants are more affordable than ionic liquids, making them appropriate for synthetic applications on a broad scale. Additionally, surfactants also have multiple properties such as being acidic, basic, neutral, cationic, and anionic. Recently, Zhang *et al.* attempted and successfully used a surfactant as a reaction solvent in synthesizing inorganic materials that possess a crystalline nature, chalcogenides and MOFs with unique structures.[29]

## Diffusion method

The synthesis is usually conducted at room temperature and does not require any external energy to carry out the reaction. During this technique, the reagents in the solution phase are layered on top of one another and are separated by a solvent layer and gradually diffused by descending physical barriers. Even in some reactions, gels are used as a medium for crystallization and diffusion. The crystals which are formed at the interface are gradually diffused to a separate layer *via* a precipitate solvent. In particular, this method is used for insoluble products. For example, MOF-5 or IRMOF-1 is obtained by diffusing $Et_3N$ into a solution of $Zn(NO_3)_2$ and $H_2BDC$ (1,4-benzenedicarboxylic acid) in DMF/chlorobenzene with a little quantity of hydrogen peroxide to aid the synthesis of $O^{2-}$ bound to the core of the SBU (secondary building unit). Recently, apart from diffusion, our group has also reported a Brønsted acid functionalized $[Co_2(\mu_2\text{-}OH)(CO_2)_2]$ that has been synthesized by utilizing secondary building units (SBUs) and employed as an electrocatalyst for the OER.[27,30,31]

## Slow evaporation method

Another method called slow evaporation, which is also similar to the diffusion method, performed at room temperature and no external energy is required. During this process, to facilitate crystal nucleation and growth, reagent solutions are combined and allowed to slowly evaporate, which forms a crystal when a critical concentration is achieved. Mostly, low boiling point solvents are used for this technique.

## Mechanochemical method

A method of creating MOFs without using solvents is called mechanochemical synthesis. The process of conducting a chemical reaction while using mechanical force is known as mechanochemistry. At room temperature, coordination bonds can be created without a solvent using ball milling or by manually grinding the reagents. Besides, one-, two-, and three-dimensional coordination polymers could be produced by adding a little quantity of solvent to the solid reaction

mixture. It is an eco-friendly method, and also we can generate materials with high purity and high efficiency in a short span of time. This method gains more interest towards the synthesis of MOFs, because it does not require any high temperature or pressure like the solvo/hydrothermal method. But major flaws are that separation of amorphous products is difficult and getting crystals is not possible by this mechanochemical method.[22,32]

## Sonochemical method

Sonochemistry is a process where molecules change chemically as a result of intense ultrasonic radiation of 20 kHz–10 MHz. When a reaction solution is exposed to ultrasonic radiation, bubbles are generated. These bubbles then produce local hot spots with high temperatures and pressure in a short lifespan, inducing chemical reactions and the rapid production of crystallization nuclei. When compared to traditional hydrothermal processes, sonochemical techniques can produce homogeneous nucleation centers and a significant reduction in crystallization time. For example, the synthesis of MOF-5 by a sonochemical method in the presence of solvent, 1-methyl-2-pyrrolidinone (NMP), yields a high-quality crystal in 30 min with a size of 5–25 micrometers.[30,32,33]

## Microwave-assisted method

A method used for the rapid synthesis of MOF based materials is the microwave-assisted method. Compared to other standard techniques, this method has some advantages, like quick and uniform heating, no selective surface heating, energy-saving process, higher yield and quicker preparation time, reduced processing cost and high purity. Even though this method cannot end-up with crystals, the microwaves aid in the mobility of the molecules, causing nucleation and production of crystals with a regulated size and shape by appropriately controlling the reaction's concentration and temperature. For example, in comparison to its traditional hydrothermal synthesis, the microwave-assisted synthesis of HKUST-1 $[Cu^3(BTC)_2(H_2O)_3]$ ($BTC^3$ = 1,3,5-benzenetricarboxylate) produced crystals with high yield and improved their physical characteristics within a shorter reaction time.[33]

## Post-synthetic method

Post-synthetic modification, or PSM, is a technique that involves adding desired functional groups to MOFs after they have been synthesized. It essentially includes transforming the MOFs chemically after they have been separated. Mostly, to synthesise isostructural MOFs with various physical and chemical properties, this technique has been used widely. The modification of the MOFs fundamental structural components involves the replacement of the secondary building unit (SBU), solvent-assisted ligand exchange or solvent-assisted linker exchange (SALE) and in some cases replacement of the metal nodes and the non-bridging ligands are examples of post-synthetic alteration. Also, bimetallic MOFs can be synthesised under this post-synthetic modification by adding second metal ions, which further increases the activity as a result of new physical and chemical properties. Moreover, defect rich MOFs can be produced as a result of the post-synthesis modification process *via* partial replacement of metal anodes or by missing or partially replacing organic linkers. The modified and functionality engineered MOFs are effectively employed in catalysis, gas sorption & desorption, separation and storage, and magnetic and luminescent applications.[30]

## MOFs as an electrocatalyst for the oxygen evolution reaction (OER)

For over a decade, MOF materials have gained vast attention as an electrocatalyst for the OER, due to their exceptional properties, like tuneable pore size, unique surface morphology, high surface area, varied chemical compositions and fascinating optical and physical properties.[34] Despite the above features, MOFs have poor stability in highly polar solvents, particularly in water, which restricts them from being widely used in OER electrocatalysis. To overcome these flaws, researchers have employed MOF derived materials (highly robust nature) like ZIFs (Zeolitic-Imidazole framework), University of Oslo (UiO), and Materials of the Institute Lavoisier (MIL) as efficient electrocatalysts for the OER.[35–39] MOFs can be employed as OER electrocatalysts directly, since they combine the advantages of homogeneous and heterogeneous catalysts.[40] However, since the majority of MOFs are created as bulk powders, their electrochemical response is hampered by poor electrical conductivity brought about by the inherent insulating abilities of organic ligands and by the insufficient overlapping between the p- and d-orbitals of metal ions. Apart from those pros, blockage of the porosity in bulk MOFs restricting the mass permeability and the obstruction of metal sites by organic ligands are both inevitable constraints on their OER performance. So, to overcome these drawbacks, researchers have tried converting a bulk structured MOF into a thin layer of MOF in a nano-regime. These thin layered MOFs possess a way to access more number of active sites and result in a higher OER performance. Upon creation, thin layered MOFs have several advantages, like facilitating excellent and quick mass transport of electrons during the OER process, exhibiting more surface area providing active sites for the conversion of $O_2$ molecules, and acting as desirable reaction substrates that can easily interact with the coordinatively unsaturated metal centres.[17,41–43]

For instance, Wang and co-workers designed 2D ultrathin NiFe-MOF nanosheets (NiFe-UMNs) using ultrasonication with a uniform thickness of ~10 nm. In contrast to bulk NiFe-MOFs, the ultra-sonicated NiFe-UMNs needed an overpotential of 260 mV to reach a 10 mA $cm^2$ current density. The NiFe-UMNs were shown to have outstanding OER catalytic activity, and this was ascribed to their ultrathin nature, which provides more number of surface coordinatively unsaturated metal sites

 

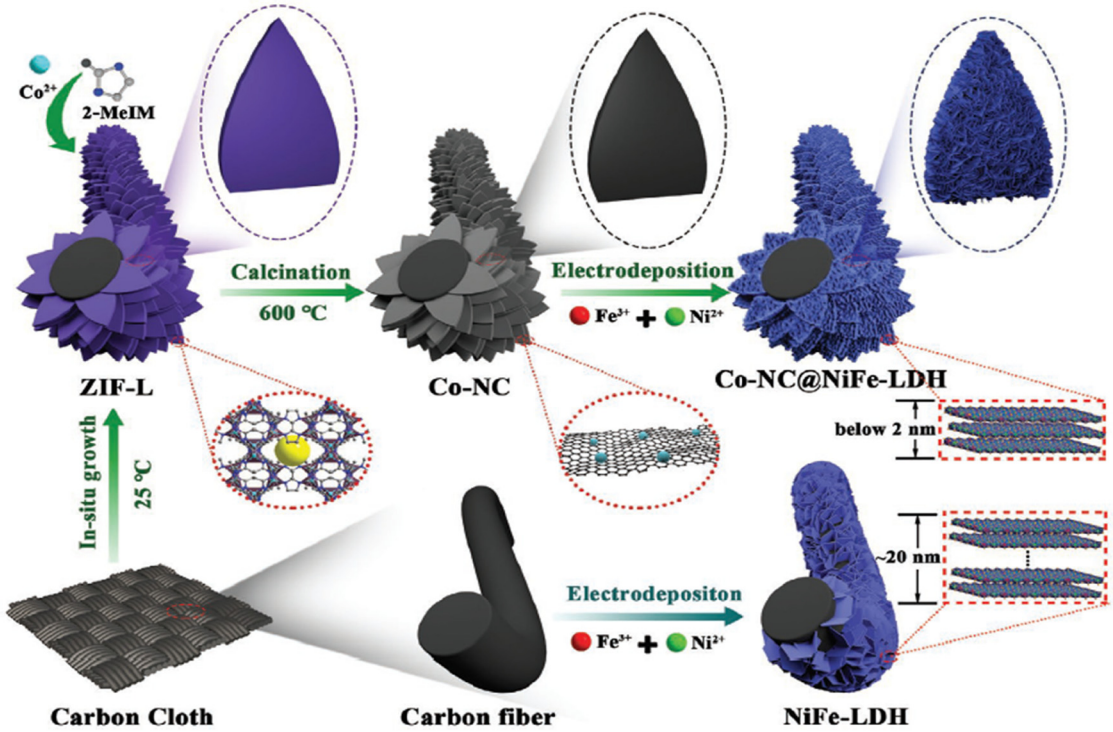


Fig. 1 Graphical representation of the synthetic processes of pristine NiFe-LDH and 3D hierarchically grown Co-NC@NiFe-LDH over carbon cloth. Reprinted with permission from ref. 45. Copyright (2021) Wiley-VCH.

and also facile electron and mass transit.[41] From the DFT calculations they found that the adsorption of $OH^-$ towards the Ni sites requires a Gibbs free energy of 1.76 eV, but at the Fe site 1.58 eV is required implying that Fe will be a better active site than Ni. Combination of these two metals will greatly reduce the energy barrier and enhance the OER activity. As evidence, XPS analysis showed that the formation of the bimetallic case leads to higher valence state of Ni sites, which dramatically speeds up the electron transfer between $OH^-$ and NiFe-UMNs by enhancing the OER activity. Moreover, Huang and co-workers developed a Cobalt pillar-layered MOF by making use of a pillar ligand with a redox active backbone that can be specifically removed and electrochemically oxidized during the OER at pH = 13. The obtained 3D Co-MOF was subjected to electrochemical exfoliation resulting in ultrathin 2D Co-MOF nanosheets of thickness 2 nm. These ultrathin 2D Co-MOF nanosheets exhibit an electrocatalytic activity with 211 mV as the overpotential to attain a current density of 10 mA $cm^{-2}$.[44] The above two methods are typically expensive, and require a long time and some solvents are toxic to the environment. For the time being, electrodeposition is thought to be an incredibly quick, efficient, and clean way to create LDHs. For instance, Shen *et al.* reported a controllable ultrathin NiFe-LDH nanoarray for effective overall water splitting, with an average thickness of less than 2 nm on MOF-derived Co-NC microarrays. By simply controlling the electrodeposition time, the Co-NC microarrays can offer more nucleation sites, which will help the formation of ultrathin NiFe-LDH with abundant oxygen vacancies and coordination of unsaturated sites. The improved Co-NC@$Ni_2$Fe-LDH shows the lowest cell voltage of 1.55 V to achieve 10 mA $cm^{-2}$ current density for total water splitting in alkaline medium. This high performance of Co-NC@$Ni_2$Fe-LDH might be due to the existence of a large number of oxygen vacancies, number of exposed active sites, reduced ion diffusion distance, excellent conductivity, and potential interactions between the Co-NC nanostructure and NiFe-LDH species, as seen in Fig. 1. By adapting this flexible technique, a variety of alternate Co-NC@ bimetal-LDHs nanoarrays with excellent uniformity and thicknesses ranging from 1.5–1.9 nm can be fabricated.[45] Although, the extraction of nanosheets from the MOF *via* the exfoliation method is only suitable for layered MOFs possessing weak interlayer interaction. Apart from exfoliation, another method called the hydrothermal method was also employed to prepare ultrathin 2D MOFs. Recently, Pang *et al.* adopted a one-step facile hydrothermal method to synthesise a 2D Co-MOF by using polyvinylpyrrolidone (PVP) as a surface directing agent.[46] They obtained a nanosheet with a thickness of ~2 nm, which displays high activity with low onset potential compared to the micro-regime structure in alkaline medium. The higher OER activity of 2D Co-MOF is due to the unsaturated $Co^{2+}$ centre for easy access of $OH^-$ reagent. Despite these advantages, the complete removal of the organic surfactant is a tedious process and even some of the surfactants will adhere to the 2D MOF nanosheets, which partially hinders the active areas.[47]

To avoid the use of organic surfactants, Lie and co-workers developed 2D CoFe-MOF nanosheets derived from the CoFe-LDH with the addition of benzene dicarboxylic acid (BDC) at

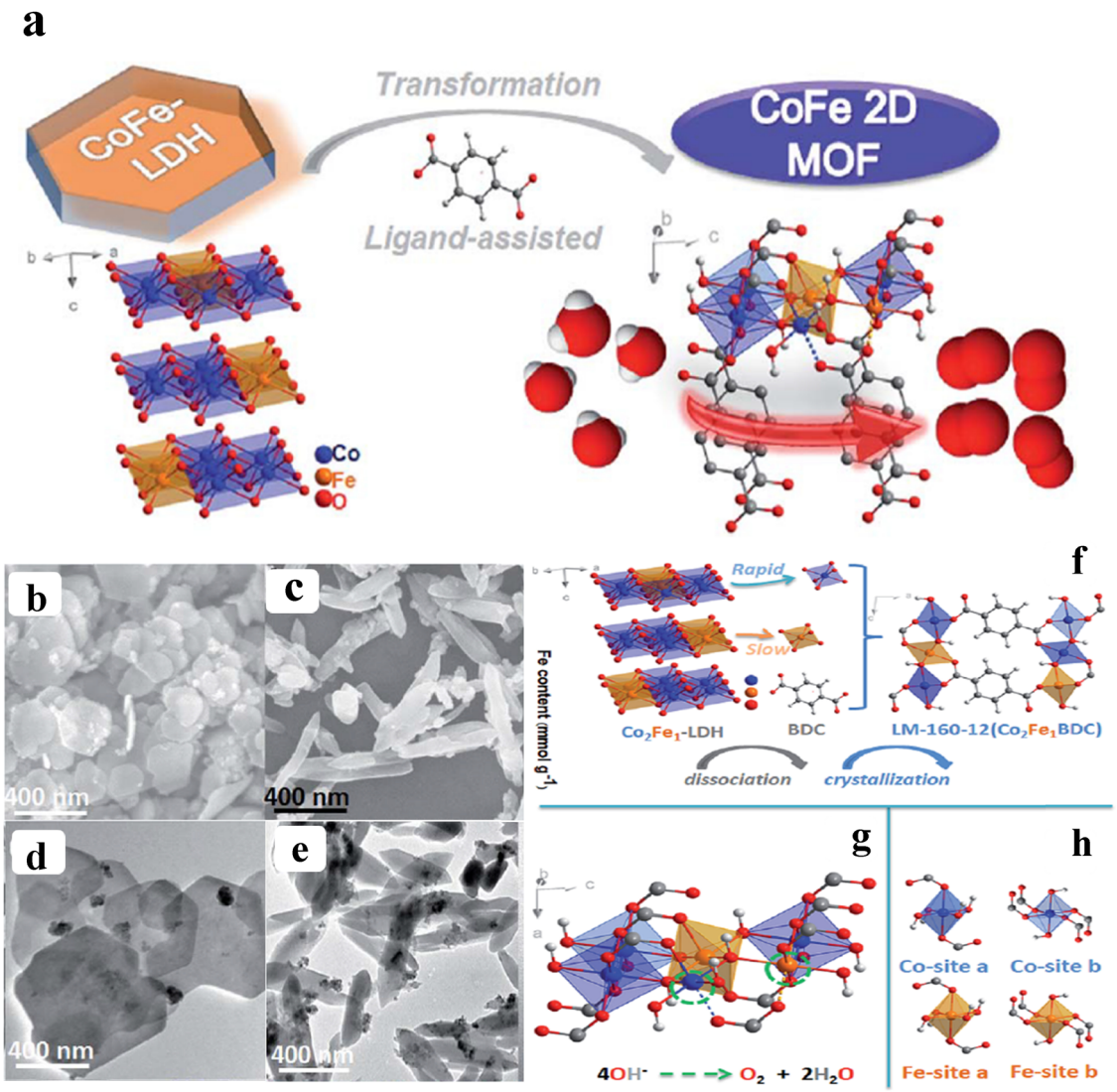


Fig. 2 (a) Schematic representation of the ligand assisted synthetic process of 2D-MOFs. (b–e) SEM and TEM images of SEM images of CoFe-LDH and LM-160-12; (f) The graphic representation of the structural change from LDHs to 2D MOFs; (g) The local unsaturated model (green dashed circle) for the metals on LM-160-surface 12's; (h) Four different pairs of [$MO_6$] octahedra. Reprinted with permission from ref. 48. Copyright (2020) Royal Society of Chemistry (RSC).

different temperatures and times in DMF medium (Fig. 2a). These nanosheets showed an excellent electrocatalytic activity of 274 mV overpotential to attain a benchmark current density of 10 mA $cm^{-2}$. From the SEM (scanning electron microscope) images Fig. 2b and c, it is observed that the hexagonal shape with a lateral diameter of 50–500 nm is transformed to spindle-like structure, owing to the presence of more active sites, and an increase in the electronic conductivity and the availability of nanosheets with a thickness of 4.84–7.39 nm after treating with the BDC for 12 h at 160 °C. The same was evident from the HR-TEM (high-resolution transmission electron microscope) images from Fig. 2d–f.[48] According to the ICP-MS analysis, cobalt nucleation proceeded more quickly than iron at first, indicating that the BDC ligand had a stronger propensity to coordinate with cobalt in the early stages of heterogeneous nucleation with the optimum condition (160 °C, 12 h). These results evidence that the parent CoFe-LDH possesses regulatable release of cations for the ligand-assisted transformation. From Fig. 2g, it can be seen that 2D bimetal layers, made of pseudo-octahedral [$CoO_6$] and [$FeO_6$] complexes, were separated along an axis by BDC ligand molecules. Hence, the four-electron route for the OER was provided by the unsaturated metal sites on the surface of LM-160-12 (green dashed circle) (Fig. 2h). However, four sets of quasi octahedral [$MO_6$] were produced using various metal centres and oxygen-containing ligands, as seen in Fig. 2i.[48] Recently, Shichun *et al.* developed trimetallic FeCoNi 2D MOF nanosheets with oxygen vacancies by a simple one pot hydrothermal synthesis. The oxygen defect-rich FeCoNi-MOFs possess a high catalytic activity with an overpotential of 254 mV to reach a 10 mA $cm^{-2}$ current density along with long-term/static durability for 100 h in an alkaline medium. The DFT study revealed that d-band

 

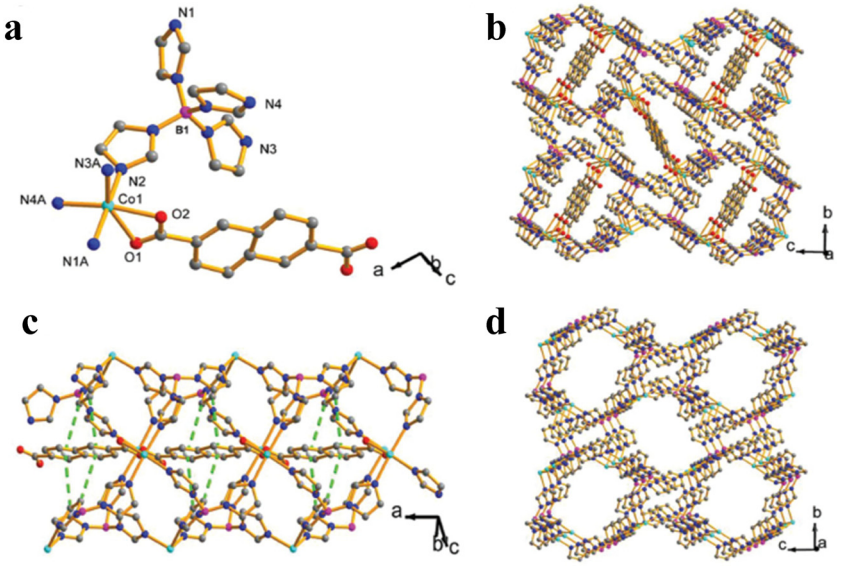


Fig. 3 (a) Self assembled BIF-91's framework coordination environment of Co(II); (b) 3D model of the BIF-91 framework; (c) effect of C–H interactions on ndc acidic ligand stabilization; (d) BIF-91's simplified Zeolitic framework in the absence of flexible auxiliary linkers. Reprinted with permission from ref. 51. Copyright (2019) Wiley-VCH.

centre is shifted away from the Fermi level, resulting in the occupation of lower antibonding states with the adsorbent ($OH^-$), which reduces the $OH^-$ adsorption Gibbs free energy and makes the OER facile with low onset potential.[49] Zhu and co-workers adopted a surfactant-free strategy to synthesize iron–cobalt MOF-74 ultrathin 2D nanosheets (FeCo-MNS) with a thickness of 2.6 nm *via* the hydrothermal method by using amorphous iron–cobalt oxide nanosheets (FeCo-ONS) as a sacrificial template. In this method, the FeCo-ONS not only acts as a metal donor for the MOFs but also acts as a template for the constrained growth of MOFs into 2D structures.[50] The aforementioned examples motivate the further design of transition-metal-based ultrathin 2D MOF nanosheets with metal derivatives as excellent templates/precursors.

## Modulating the electronic structure of MOFs

Despite the flaws of ultrathin MOF fabrication, controllably modifying the bulk structure of MOFs with precisely tweaking their characteristics will beneficially improve the activity of the OER process. For instance, Qiao *et al.* reported a new Co-based red-block crystal of $CoB(im)_4(ndc)_{0.5}$ (BIF-91 = boronimidazole framework, im = imidazolate, ndc = 2,6-naphthalenedicarboxylate), a rigid electrocatalyst for the OER in 1 M KOH. The naturally occurring carboxylate species in the BIF system provides multiple domains, which will adopt the ndc ligands as a result of zeolite channel confinement. Also, the rigidity of the framework is due to even distribution of 3/4-connected boron components. In particular, the BIF-91 molecular channel porosity was reduced with the increase in the density of the coordination bonds as a result of the incorporation of bridging ndc ligands. The incorporation of ndc ligands will keep the crystallinity of the BIF-91 in alkaline solution, and also the presence of the conjugated system would favour the atomic level adsorption of $Fe^{3+}$ and $Co^{2+}$ ions and further increase the electrocatalytic activity too. The crystal structure obtained from single-crystal X-ray diffraction is provided in Fig. 3a, where each $Co^{2+}$ centre adopted a $CoN_4O_2$ distorted octahedral coordination geometry, which was bridged by 2 O atoms and 4 N atoms in the $B(im)_4^-$ ligands. Also, the coordination site 5 and 6 is bonded with $ndc^{2-}$ and $B(im)_4^-$ ligands like a 3D network (Fig. 3b). As mentioned above, the stability of BIF-91 is increased by the interactions of C–H–π with the $ndc^{2-}$ and $B(im)_4^-$ ligands (Fig. 3c). Interestingly, Fig. 3d looks like an eight-membered ring molecular sieve ($\approx 9.9 \times 14.4$ Å) formed by the redundant bonds of bridging ndc acid ligands.[51] Another work by Guodong *et al.* prepared a durable NiRu-MOF, grown on Ni-Foam by using 2,5-thiophenedicarboxylic acid as an organic linker *via* a simple hydrothermal method. In this approach, the electronic structure of Ni-MOF is altered by doping of $Ru^{3+}$ ions. The XPS analysis evidenced that after doping of Ru towards Ni-MOF, the binding energy of Ni 2p is shifted to 0.2 eV positively. Also, XANES (X-ray absorption near-edge structure) analysis shows the increased photon energy in the Ru-doped Ni-MOF compared to the bare Ni-MOF. These XPS and XANES results confirmed the reduced local electron density of Ni sites and which will act as electron donors. According to DFT studies, $NiRu_{0.08}$-MOF was found to have a better conductivity and possess a lower adsorption energy for intermediates during the OER process and exhibited a much lower overpotential of 187 mV to reach a current density of 10 mA $cm^{-2}$.[52] On the other hand, a unique strategy was adopted by Jiang and co-workers for tuning the electronic structure of the Ni based MOF *via* a simultaneous incorporation of ($Fe^{3+}$) metal

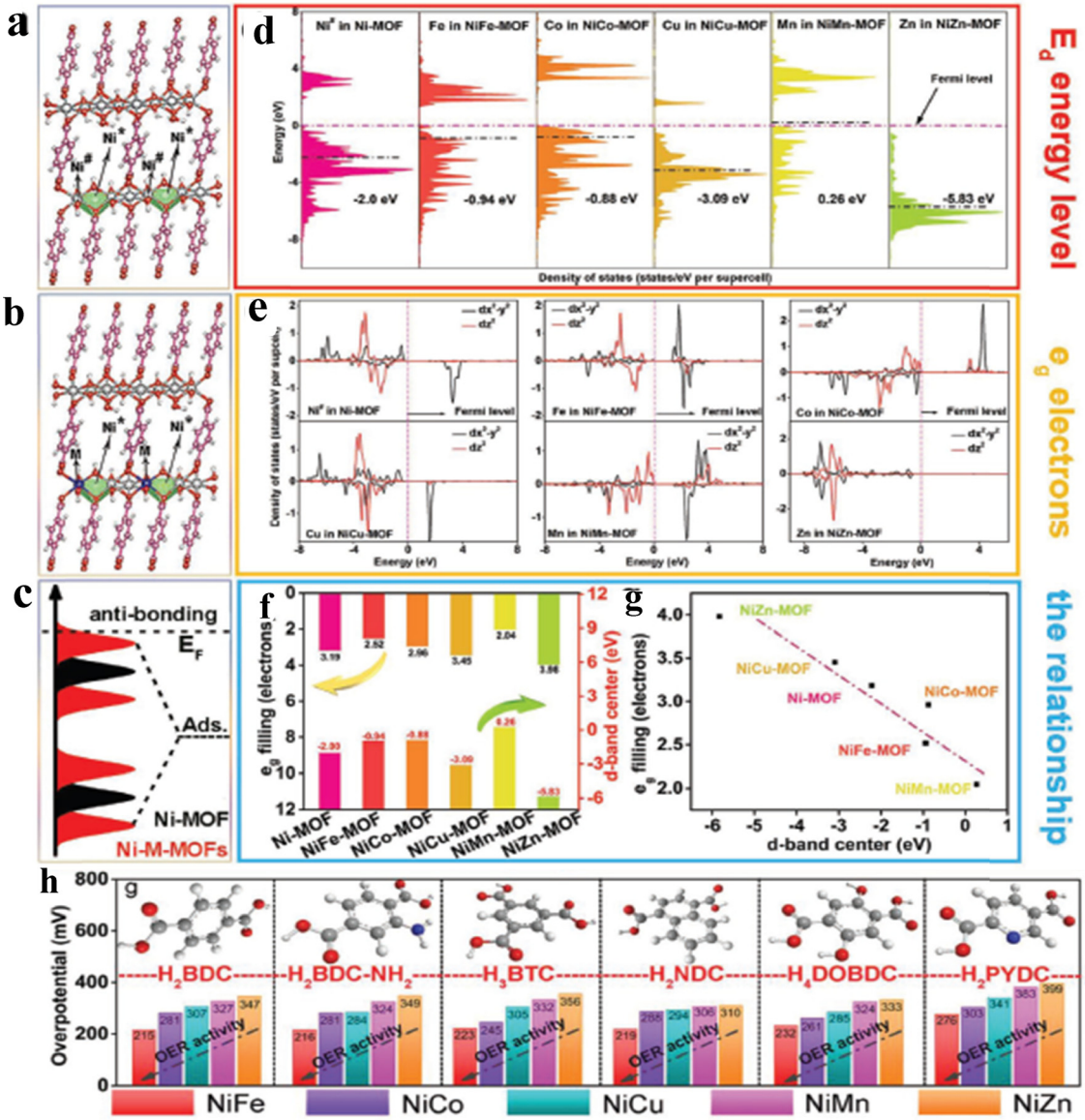


Fig. 4 (a and b) Optimized crystal structure of Ni-MOF and Ni-M-MOFs; (c) schematic design of bond formation between the catalyst and the adsorbate; (d and e) projected d-orbital and $e_g$ density of states of M in Ni–M-MOFs (M = Fe, Co, Cu, Mn, and Zn); (f) corresponding bar diagram of the calculated d-band center ($E_d$) and $e_g$ filling ($f_e$) for substituted M in Ni–M-MOFs; (g) OER activity trend of Ni–M-MOFs while using different organic linkers. (h) Comparison of overpotential required for $j$ = 10 mA cm$^{-2}$ of different MOF-based catalysts with the use of different ligands in the synthesis process. Reprinted with permission from ref. 54. Copyright (2021) Wiley-VCH.

ions and counter ions ($BF_4^-$) by using $Fe(BF_4)_2{\cdot}6H_2O$ as a source under stirring conditions. The DFT calculations suggest that for the optimized NiFe-MOF-$BF_4$-0.3 NSs, the electron density near the Fermi level was increased, thus providing higher conductivity and improving the catalytic activity. Furthermore, $\Delta G$ for the formation of *OOH intermediates (Rate determining step) is reduced to 1.45 eV after the incorporation of $Fe^{3+}$ and $BF_4^-$ ions (M–F interaction) compared to the NiFe-MOF NSs. Moreover, the DFT calculated overpotential of the NiFe-MOF-$BF_4^-$-0.3 NSs (0.25 V), Ni-MOF NSs (0.56 V) and NiFe-MOF NSs (0.41 V) follows the same activity trend as the experimental overpotential.[53] To further study the relationship between electronic structure and catalytic activity, Heqing *et al.* fabricated a series of bimetallic Ni-based metal–organic frameworks (Ni–M-MOFs, M = Fe, Co, Cu, Mn, and Zn) with definite morphology and active sites. In this case, the periodic structural units contain two different Ni sites of coordinately saturated metal centres ($Ni^{\#}$) and unsaturated metal centres (Ni*), seen in Fig. 4a. During the OER process, Ni* species are typically exposed on the catalyst surface and serve as the active sites to interact with the intermediates. By using DFT calculation and partially substituting the $Ni^{\#}$ with the transition-metal atoms M (M = Fe, Co, Cu, Mn, and Zn) to the Ni-MOF, violation of the electronic structure will be studied

 

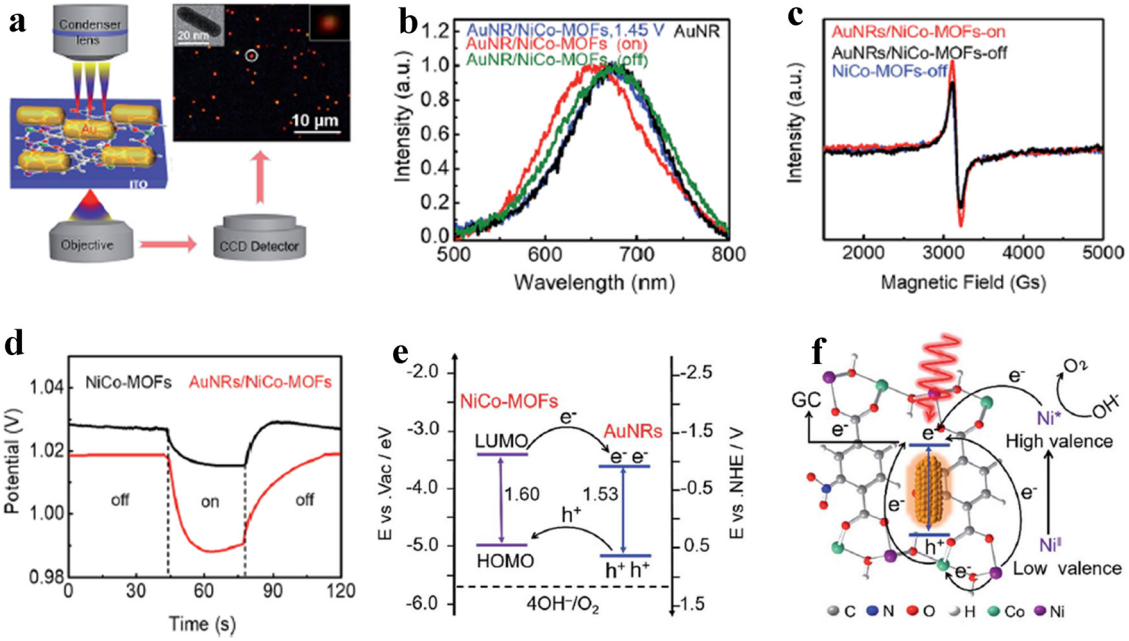


Fig. 5 Monitoring of hot charge carrier transfer between Au NRs and NiCo-MOFs, with the integrated electrochemical technique coupled with dark-field spectroscopy. (a) Dark field image of the deposited Au nanorods over the substrate; (b) LSPR scattering spectra; (c and d) EPR spectra and open circuit potential *vs.* time curves of Au NRs/NiCo-MOFs and NiCo-MOFs with and without light; (e) the energy level diagram representing the transfer of electrons between Au NRs and NiCo-MOFs upon 808 nm light irradiation; (f) corresponding electron transfer pathways between Au NRs and NiCo-MOFs. Reprinted with permission from ref. 56. Copyright (2019) Royal Society of Chemistry (RSC).

(Fig. 4b). The d-band centre and projected density of states (PDOS) in Fig. 4c and d showed that NiFe-MOF possesses a moderate value for adsorption/desorption of oxygen-containing intermediates O*, OH*, OOH*, and OO* during the OER process. The d-band centre ($E_d$) and electrons filling in the $e_g$ orbitals exhibit a linear relationship with one another (Fig. 4e and f), suggesting a comparable physical mechanism for regulating the OER activity. Moreover, the accuracy of the strategy was tested by modifying the organic ligands alone with the same metallic composition. Here also, they found the same aforementioned activity trend of NiFe-MOF > NiCo-MOF > NiCu-MOF > NiMnMOF > NiZn-MOF (Fig. 4g). In addition, from Fig. 4a–g, it is seen that NiFe-MOF showed the best catalytic activity even with various organic ligands in 1 M KOH electrolyte.[54] As mentioned, the poor electro-conductivity of MOFs such as ZIF-67 limited their practical applications. So, to enhance the conductivity of ZIF-67, Hou *et al.* decorated HTTP (2,3,6,7,10,11-hexahydroxytriphenylene), a π-conjugated molecule, by a simple hydrothermal method at different reaction times. The decorated π-conjugated molecule HTTP will directly accelerate and enhance the electron transfer during the OER process. As a result, charge transfer resistance is significantly reduced with a high catalytic activity of 238 mV at 10 mA $cm^{-2}$ current density. Hence, the use of aromatic π-conjugated ring molecules will greatly help the electron transfer and boost the OER process.[55] In some cases, for accelerating the OER process, activation of NiCo-MOF *via* Au nanorod plasmons was employed. Here, plasmon generated hot charge carriers are inserted into the NiCo-MOF network leading to considerable increases in the valence state of active Ni species, which in turn reduces the activation energy of the OER. The hot charge carrier passage between Au NRs and NiCo-MOFs was directly examined using the electrochemical technique that included dark-field spectroscopy. The dark-field picture in Fig. 5a shows the Au NRs as red coloured dots. In addition, due to the difference in dielectric constant, the LSPR (Localized surface plasmon) bands of Au NRs are negatively shifted to 668 nm from 674 nm upon being hybridised with NiCo-MOFs (Fig. 5b). Also, the blueshift of ~23 nm was observed after 30 min illumination of light, which might be due to the increase in electron cloud of Au NRs. Moreover, with EPR analysis, they tried to find any difference in the paramagnetic signal at 3155 Gs corresponding to the Ni ion and the difference was negligible. On the contrary, a significant difference in the EPR signal was observed upon illumination of light, as seen from Fig. 5c. The measurement of $V_{oc}$ *vs.* light irradiation in Fig. 5d showed a negative shift of 30 mV corresponding to the accumulation of hot charge during irradiation. The plasmon enhanced OER mechanism evidenced that the abundance of hot holes and strong electronegativity of Au NRs allowed the electrons to transfer from the NiCo-MOFs lowest unoccupied molecular orbital (LUMO) to the Au NRs highest occupied molecular orbital (HOMO) (Fig. 5e). Fig. 5f shows the two possible electron transfer pathways from Au NRs to NiCo-MOFs under irradiation of light at 808 nm. As a result, the activation energy of NiCo-MOFs is reduced and enhances the OER process.[56] Guo and co-workers reported a non-destructive and selective modification of metal sites in the MOF network *via* low-temperature (LT) air

plasma.[57] This approach provides highly reactive oxygen species, such as atomic oxygen and oxygen molecules in excited states. LT air plasma treatment produces a highly stable and active framework of Co-Prussian analogue with deficient ferricyanide units. Reactive oxygen species produced from the LT air-plasma cause oxygen to bond to Co's open sites, which accelerates Co's oxidation state to $Co^{3+}$, an active site for the $O_2$ molecules conversion with an overpotential of 330 mV. Another interesting work by Sharath *et al.* reported a novel method of designing a chemically stable squarate based bimetallic NiFe-MOF with zbr topology as an electrocatalyst for the OER. By simply tuning the $Ni^{2+}$ content over the bimetallic MOF, they have reported a series of NiFe-MOF electrocatalysts. The optimized electrocatalyst $Ni_2Fe_1$ Sq-zbr-MOF shows a low overpotential of 230 mV (at 10 mA $cm^{-2}$) in 1 M KOH solution.[58] The aforementioned works motivated the researchers to develop/fabricate various electronically modified MOF networks as efficient electrocatalysts for the OER.

## Self-supportive/*in situ* grown MOF-electrocatalyst

As of now, a number of techniques have been employed to modify the morphologies, chemical compositions, and electronic structures of the MOF-based electrocatalysts. Despite the outstanding performance towards the OER, most of the MOFs are powder-based electrocatalysts. The direct use of powdered MOFs for electrocatalytic applications is very difficult without the use of any polymeric binders like Nafion, polyvinylidene fluoride (PVDF) and polytetrafluoroethylene (PTFE).[59–61] Polymeric binders may, however, result in partial masking of the active sites and obstruction of mass movement at the catalyst–electrolyte interfaces.[62] Therefore, it is highly desired to fabricate electrodes using self-standing, binder-free MOFs. In 2020, Zhigang *et al.* developed a novel MOF-derived carbon encapsulated $CoS_2$ nanoarray for efficient electrocatalytic OER in alkaline medium. When compared to $CoS_2$@NF and other counter catalysts, the MOF-derived NGC (N-doped graphitic carbon) not only offers more effective active sites but also improves the operational stability. Fig. 6a shows a schematic representation of the synthesis of $CoS_2$@NGC@NF. The SEM images (Fig. 6b–g) show the morphology of nanowires, wrapped pimple-shaped skin and wrinkle rod-like morphology of $CoS_2$@NGC@NF. This approach shows high catalytic activity with an overpotential of 243 mV with a lowest Tafel slope value of 71 mV $dec^{-1}$. Even at higher current density also, $CoS_2$@NGC@NF exhibits a high current density of 105.1 mA $cm^{-2}$ with an outstanding stability for 20 h. As the work function variation at the $CoS_2$–C layer interface causes an electron-poor NGC shell with a significant decrease in the carbon Fermi level, the core–shell $CoS_2$@NGC hybrids vastly improve the interfacial electron transfer, lowering the barrier for electrons to move from adsorbed OER intermediates to carbon active centres. Doping of *p*-type, like pyridinic N in graphene carbon, benefits the reduction of the carbon Fermi level in graphene which results in a smaller energy gap between the C–O σ state and the carbon Fermi levels and a reduced kinetic barrier for the OER (Fig. 6h).[63] In addition, Biradha *et al.* fabricated a binder free Mn-MOF as a 3D electrode *via* freshly synthesized tetracarboxylic acid by a solvothermal treatment at 100 °C for 24 h. The electrochemical studies of the OER demand a 280 mV overpotential to reach 10 mA $cm^{-2}$ with a remarkable stability. The enhanced performance is significantly due to the synergistic effect between the $Mn^{2+}$ and $Ni^{2+}$ from the NF substrate. The *in situ* growth on NF exhibits more number of active species by preventing the agglomeration of the active species, and on the other hand it increases the conductivity of non-conducting electroactive species like Mn-MOF.[64] Yet another interesting work, a single-atomic Co electrocatalyst self-supported on carbon cloth (CC) was reported by Min and co-workers. The self-supported Co-single atomic electrocatalyst nanosheet arrays (SS-Co-SAC NSAs) were synthesized by simple ageing of CC in a solution containing Zn/Co metal ions and 2-methylimidazole for 2 h followed by pyrolysis at $N_2$ atm (Fig. 7a). The nanosheet array was clearly seen from the SEM analysis and also a sheet-like structure was revealed from the HR-TEM analysis (Fig. 7b–d). The atomic force microscopy (AFM) in Fig. 7e revealed that the nanosheet (SS-Co-SAC NSAs) thickness was approximately 35 nm. Moreover, the uniform distribution of Co atoms (yellow circle) was clearly seen in Fig. 7f and g. The XANES and EXAFS results in Fig. 7h and i showed that a more predominant oxidation state of Co and a strong *R*-space peak at 2.18 Å are responsible for the Co–Co coordination in the SS-Co-SAC NSAs compared to the bare ZIF-67, respectively. FT-IR (Fourier-transformed infrared spectroscopy) reveals that there is just one strong vibration band seen at 2090 $cm^{-1}$, which can be attributed to linear adsorption of CO on a single Co center for SS-Co-SAC NSAs (Fig. 7j). The obtained SS-Co-SAC NSAs showed 348 mV as the overpotential ($\eta_{10}$) in 0.1 M KOH solution (Fig. 7k).[65] Apart from the NF and CC, researchers are focusing on copper foam (CF) as a substrate for electrocatalytic applications. Recently, Jian and his co-workers fabricated *in situ* grown hierarchical $Cu_3(PO4)_2$/Cu-BDC nanosheets on a CF substrate as a superior electrocatalyst for the OER. Initially, $Cu_3(PO4)_2$ over the CF was grown by ageing with $Na_2HPO_4$ for 6 h at 40 °C. By using a solvothermal method, Cu-BDC nanosheets were grown over the $Cu_3(PO4)_2$/CF at different reaction times. The optimized $Cu_3(PO4)_2$/Cu-BDC-150-6 acts as an excellent electrocatalyst for the conversion of $H_2O$ molecules to $O_2$ with an overpotential of 241 mV to reach a 10 mA $cm^{-2}$ current density. The SEM and HR-TEM images showed perfect nanosheets, which are hierarchically grown over the CF at different reaction times (Fig. 8a–f).[66] On the other hand, in some applications like optical and photo-electrocatalytic applications, conductive supports like indium tin oxide (ITO), transparent conductive oxides (TCOs) and fluorine tin oxide (FTO) are used, because these substrates are conductive, highly transparent, and easily transmit the incident light. The creation of MOF thin films with these substrates provides greater stability, compared to powdered MOFs.[67] As a result, a comparison table of OER performance for MOF-based nanostructured electrocatalysts is

 

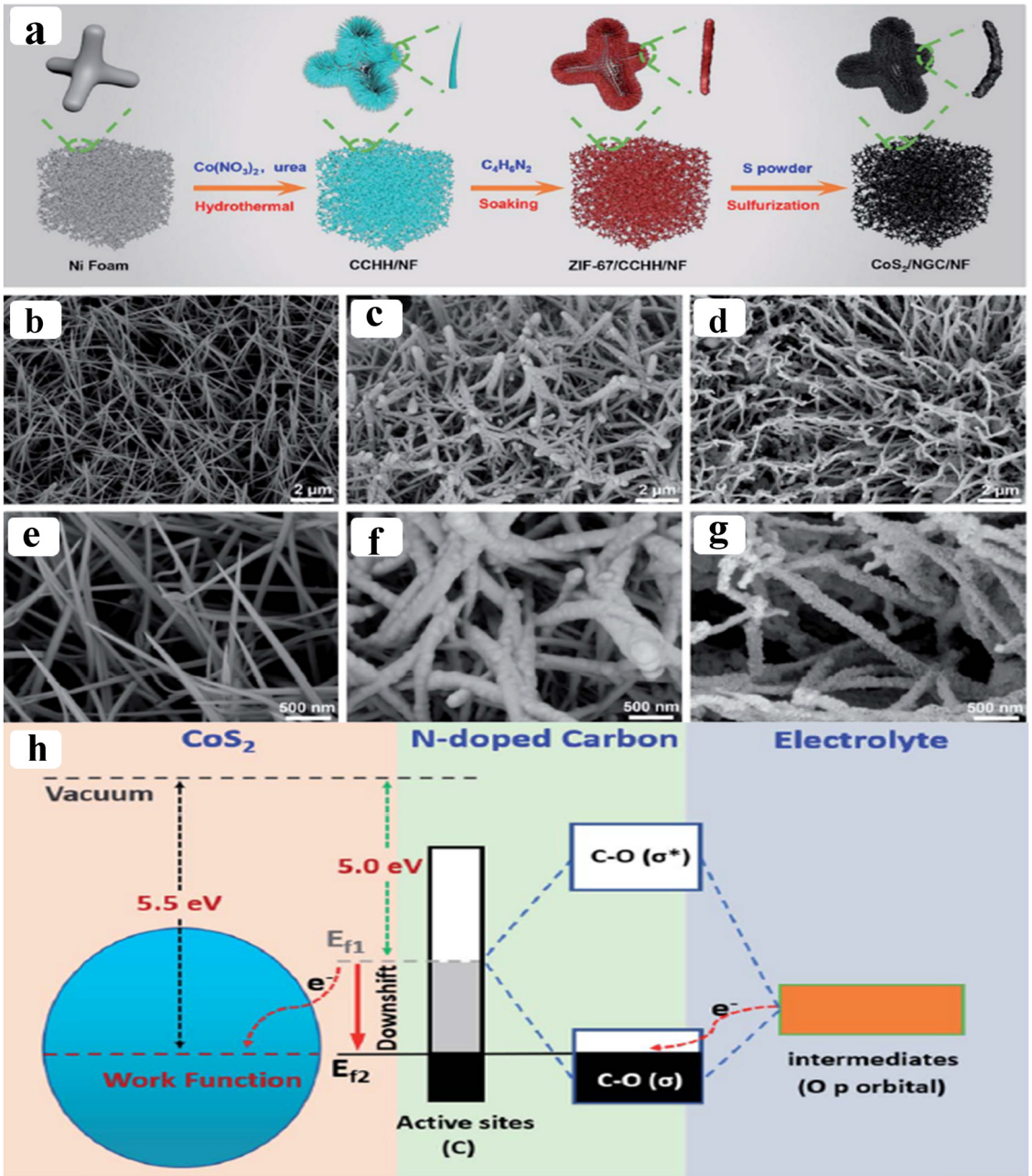


Fig. 6 (a) Schematic representation of the synthetic protocol of $CoS_2$@NGC over NF; (b and c), (d and e) and (f and g) show the SEM images of CCHH@NF, ZIF-67@CCHH and $CoS_2$@NGC over NF; (h) illustrates the downshifting of the high work function of $CoS_2$ at the Fermi level and facilitates the extraction of electrons from the O p orbitals of the adsorbed intermediates to the carbon active sites *via* the C–O s orbitals. Reprinted with permission from ref. 55. Copyright (2020) Royal Society of Chemistry (RSC).

provided in Table 1. Based on the above discussed examples, developing *in situ* or self-supportive electrodes is crucial for achieving a powerful and long-lasting water splitting reaction. The high performance of the above self-supportive/*in situ* grown electrocatalyst might be due to several factors, such as the intimate interfacial interaction between the substrate and electrocatalyst enhancing the conductivity, which will further facilitate the charge transfer kinetics; more accessible active sites being generated with high surface areas of the substrates, which leads to a high loading and uniform distribution of electrocatalysts with distinctive shape; the substrate integrated *in situ* growth of electrocatalyst avoids the post coating of the catalyst with organic binder by boosting the structural integrity and durability of the material. In summary, self-supported electrodes with *in situ* grown electrocatalysts can reduce interfacial resistance, expose more active sites, and increase robustness, compared to conventional electrodes in powdery deposition form with an external organic binder.

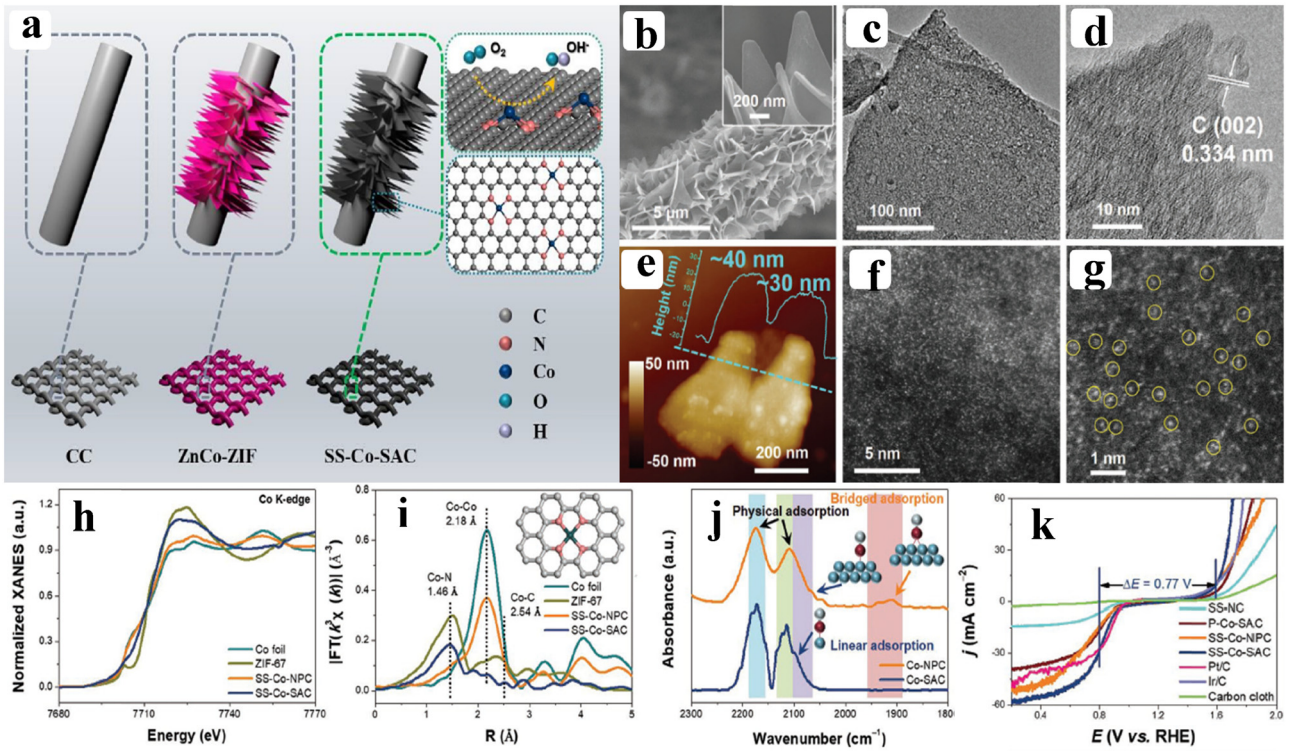


Fig. 7 (a) Schematic demonstration of the synthesis of SS-Co-SAC; (b–g) show the SEM, TEM, HRTEM, AFM, and HAADF-STEM images of SS-Co-SAC NSAs; (h and i) Co K-edge XANES and FT-EXAFS spectra of SS-Co-SAC, SS-Co-NPC, ZIF-67, and Co foil respectively; (j) *in situ* FT-IR CO absorption spectra over SS-Co-SAC and SS-Co-NPC NSAs; (k) corresponding OER and ORR polarization curves. Reprinted with permission from ref. 65. Copyright (2019) Wiley-VCH.

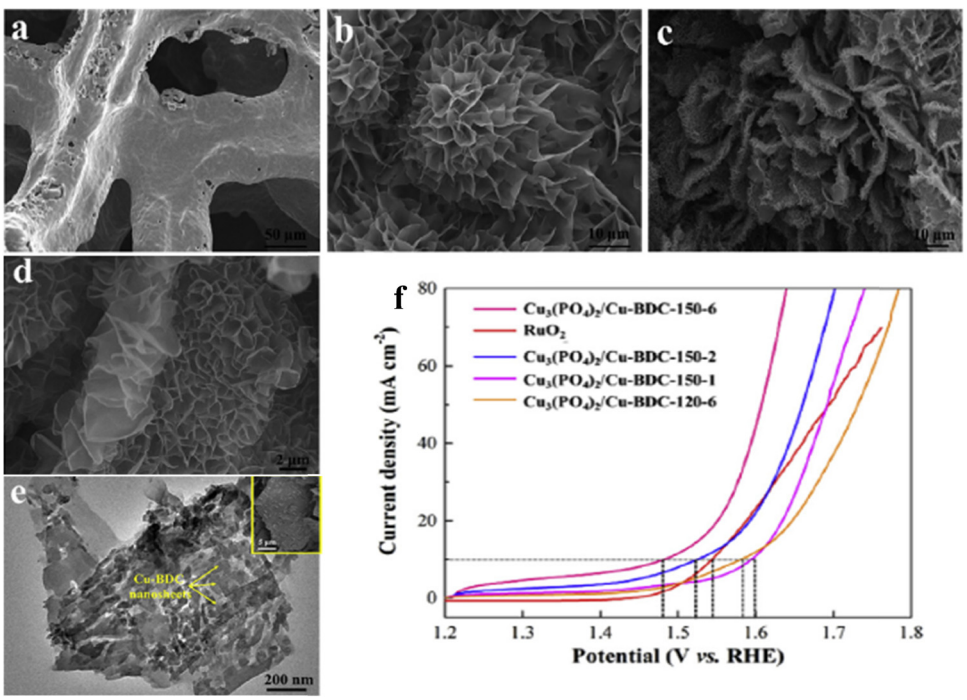


Fig. 8 FESEM images of (a) CF, (b) $Cu_3(PO4)_2$ nanosheets and (c and d) $Cu_3(PO4)_2$/Cu-BDC-150-6 foam; (e) represents the HR-TEM images of $Cu_3(PO4)_2$/Cu-BDC; (f) LSV polarization results of $Cu_3(PO4)_2$/Cu-BDC foams and commercial $RuO_2$. Reprinted with permission from ref. 66. Copyright (2019) Elsevier.

 

Table 1 A comparison of the OER performance for MOF-based nanostructures as electrocatalysts

| S. No. | Electrocatalyst | Substrate | Overpotential (mV) | Current density | Tafel slope (mV dec$^{-1}$) | Electrolyte | Ref. |
|---|---|---|---|---|---|---|---|
| 1 | Co-NC@$N_{i2}$Fe-LDH | CC | 233 | 10 mA cm$^{-2}$ | 49.1 | 1 M KOH | 45 |
| 2 | Ultrathin Co-MOF | GCE | 263 | 10 mA cm$^{-2}$ | 74 | 1 M KOH | 46 |
| 3 | LM-160-12 | GCE | 274 | 10 mA cm$^{-2}$ | 46.7 | 1 M KOH | 48 |
| 4 | FeCoNi-MOFs | GCE | 254 | 10 mA cm$^{-2}$ | 21.4 | 1 M KOH | 49 |
| 5 | FeCo-MNS-1.0 | Pt-foil | 298 | 10 mA cm$^{-2}$ | 21.6 | 1 M KOH | 50 |
| 6 | Fe@BIF-91 | GCE | 350 | 10 mA cm$^{-2}$ | 71 | 1 M KOH | 51 |
| 7 | $NiRu_{0.08}$-MOF | NF | 187 | 10 mA cm$^{-2}$ | 40 | 1 M KOH | 52 |
| 8 | NiFe-MOF-BF4-0.3 | GCE | 237 | 10 mA cm$^{-2}$ | 41 | 1 M KOH | 53 |
| 9 | NiFe-MOF | CFC | 215 | 10 mA cm$^{-2}$ | 49.1 | 1 M KOH | 54 |
| 10 | HHTP@ZIF-67 | GCE | 238 | 10 mA cm$^{-2}$ | 104 | 1 M KOH | 55 |
| 11 | AuNRs/NiCo-MOF | GCE | 240 | 10 mA cm$^{-2}$ | 69 | 1 M KOH | 56 |
| 12 | Co-PBA-plasma-2h | NF | 330 | 10 mA cm$^{-2}$ | 53 | 1 M KOH | 57 |
| 13 | MAF-X27-OH(Cu)-3 | GCE | 292 | 10 mA cm$^{-2}$ | — | 1 M KOH | 59 |
| 14 | CoFe-MOF-OH | GCE | 265 | 10 mA cm$^{-2}$ | 44 | 1 M KOH | 60 |
| 15 | $CoS_2$@NGC@NF | NF | 243 | 10 mA cm$^{-2}$ | 71 | 1 M KOH | 63 |
| 16 | Mn-MOF | NF | 280 | 20 mA cm$^{-2}$ | 31.3 | 0.1 M KOH | 64 |
| 17 | SS-Co-SAC NSAs | CC | 348 | 10 mA cm$^{-2}$ | — | 0.1 M KOH | 65 |
| 18 | $Cu_3(PO4)_2$/Cu-BDC-150-6 | CF | 241 | 10 mA cm$^{-2}$ | 76 | 1 M KOH | 66 |
| 19 | Co-MOF-5 | CC | 240 | 10 mA cm$^{-2}$ | 120 | 1 M KOH | 68 |

Where, GCE-glassy carbon electrode; CFC-carbon fiber cloth; NF-nickel foam; CC-carbon cloth; CF-copper foam.



## MOF-based derivatives as electrocatalysts for the OER

Generally, MOFs used as electrocatalysts have limitations like chemical stability and electro conductivity. To overcome these issues, MOF-derived materials are employed as electrocatalysts, which exhibit better catalytic activity towards the OER.[24] The primary divisions of MOF derivatives are metal/metal oxide-MOF hybrids, transition metal adorned porous carbons, metal oxides, nitrides, phosphides, sulfides and selenides generated from MOFs. Most of these derivatives often exhibit significant surface area and porosity by replicating the initial shape of their progenitors.

## Metal/metal oxide-MOF hybrids

Owing to the poor electrical conductivity of pristine MOFs, high catalytic efficiency towards OER performance was not achievable. These flaws can be overcome by the functionalization of pristine MOFs with metal/metal oxide nanoparticles.[69–71] The functionalization of MOFs will possess suitable adsorption energies for adsorbed oxygen ($O_{ads}$), opening the door for high-performance OER electrocatalysts *via* a synergistic effect and interfacial interaction between the MOF and metal/metal oxide nanoparticles. Subsequently, Xiao *et al.* reported $Co_3O_4$/Co–Fe oxide double-shelled nanoboxes (NBs) synthesised *via* an anion exchange reaction between ZIF-67 nanocubes (NCs) and $[Fe(CN)6]^{3-}$ ions (Fig. 9a). From the SEM and HR-TEM results, double shelled nanoboxes of $Co_3O_4$/Co–Fe oxide (DSNBs) are seen in Fig. 9b–g. The $Co_3O_4$/Co–Fe oxide DSNBs delivered high catalytic activity with a lower over potential of 297 mV to reach 10 mA cm$^{-2}$ (Fig. 9h). In this strategy, the doubled shelled nanoboxes not only provide large exposed active sites but also enhance the interface area between the electrode–electrolyte interfaces towards the high performance OER.[72]

Another strategy called the partial pyrolysis technique creates highly active nanoparticles while maintaining the MOF's framework structure for efficient substrate transport. Through the use of a partial pyrolysis technique and NiCoFe-MOF-74 as a semi-MOF precursor, Li *et al.* created sturdy NiCo/$Fe_3O_4$ heteromolecules enclosed with MOF-74 (NiCo/$Fe_3O_4$/MOF-74). The results of ETEM (environmental transmission electron microscope) under $N_2$ atm evidence the partial pyrolysis behavior of NiCoFe-MOF-74. The NiCoFe-MOF-74 and various temperature pyrolyzed MOF-74 at different time intervals delivered a distinct catalytic activity towards the OER process. DFT studies also evidenced that after formation of the heterostructure the free energy for adsorption of $OH^-$ is reduced compared to the pristine MOF-74.[73] Apart from the modification through metal oxides, recently, Cheng *et al.* reported a modification of the electronic structure of Co-MOF through inter-doping of platinum group-element ruthenium (Ru) over the CC. The formed Ru–Co MOF nanosheets are transformed into a unique hollow nanosheet of (Ru–Co)$O_x$ by annealing at 300 °C. The results of SEM analysis evidence the hollow structure of (Ru–Co)$O_x$. The positive shifting (0.74 eV) of binding energy observed from XPS indicates the alteration of the electronic structure after the ion-exchange process of $Ru^{3+}$ ions with Co ions. This positive shifting displays the electron deficient Co ions, which will moderately adsorb the $OH^-$ ions and facilitate the OER process with out-standing activity of 171.2 mV overpotential at 10 mA cm$^{-2}$.[74] Also, recently from our group, Co-BTC derived Co–$RuO_2$ nanorods were reported through the same ion-exchange process and employed as pH-universal OER electrocatalysts. In this study, after doping of $Ru^{3+}$, we observed a change in the electronic configuration of Co 2p *via* XPS analysis. The change in electronic structure makes Co electron deficient, which further serves as an active site for the $OH^-$ adsorption.[75] Furthermore, the above discussion evidences that the fabrication of a heterogeneous nanointerface has recently been recognized as an effective method for influencing the valence

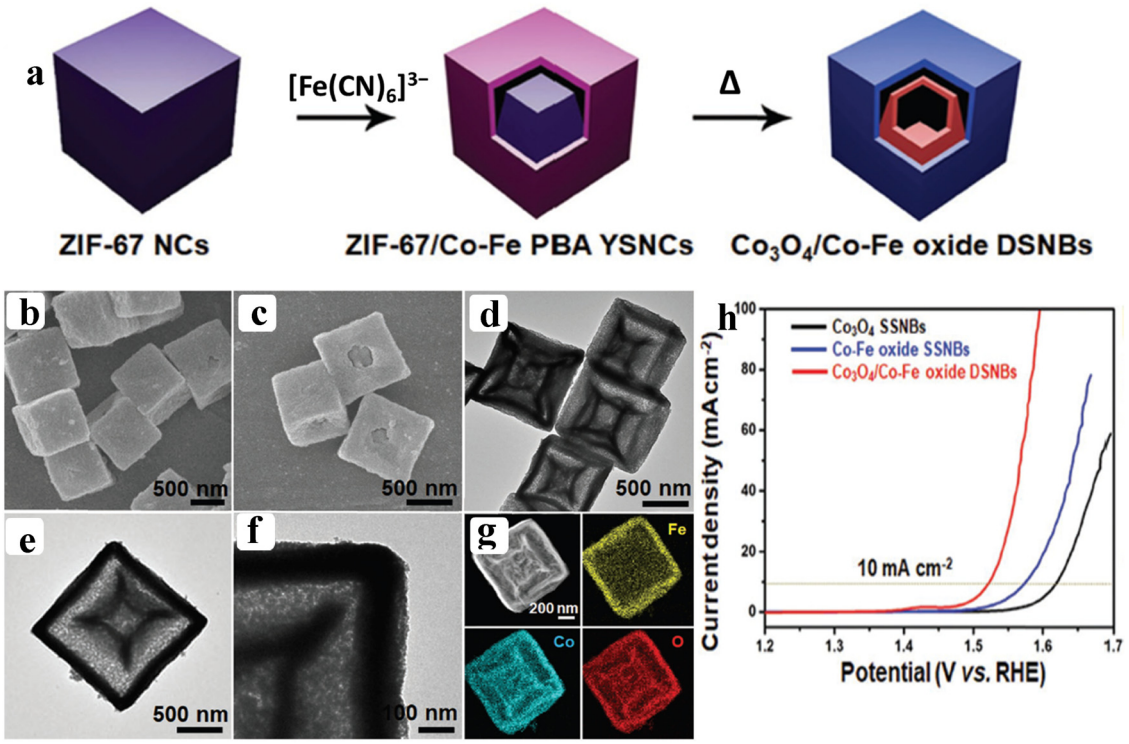


Fig. 9 (a) Schematic representation of the formation process of $Co_3O_4$/Co–Fe oxide DSNBs; (b and c) and (d–f) show the FE-SEM and HR-TEM images of $Co_3O_4$/Co–Fe oxide DSNBs, respectively; (g) corresponding HAADF elemental mapping results; (h) LSV outcomes of $Co_3O_4$/Co–Fe oxide DSNBs, Co–Fe oxide SSNBs, and $Co_3O_4$ SSNBs. Reprinted with permission from ref. 72. Copyright (2018) Wiley-VCH.

electron state of active sites and exerting an interfacial synergy effect, towards the enhancement of the OER process.

## Metal–carbon materials derived from MOFs

Due to the unique structural properties, MOF derived porous carbons and metal/metal oxide porous carbon materials are synthesized by annealing/pyrolysis at high temperature in a $H_2$/$N_2$/Ar atmosphere. During the annealing/pyrolysis process, the composition of the pristine MOF is completely decomposed, which convert the metal ions into metal/metal oxide which is embedded in the porous carbon matrix created from the organic ligands. The MOF derived carbon materials have gained more interest in water splitting applications, due to possessing several advantages compared to the pristine MOFs, like high porosity; high surface area; conductivity being greatly enhanced by high conductive nano-carbons; providing more active sites; due to customizable compositions of MOFs, a range of heteroatoms, including B, N, P, and S, are doped into the porous carbons; and different morphologies could be achievable.[76] For instance, Thangjam and co-workers reported a freestanding, defect-rich Fe–Co–O/Co metal@N-doped carbon (Co@NC) mesoporous nanosheet (mNS) heterostructure on Ni foam through annealing for 800 °C under Ar atm followed by *in situ* oxidation *via* CV cycling (Fig. 10a). The FE-SEM analysis shows the reconstruction of nanospikes (Fe–Co–O/Co@NC/NF) to nanosheets (Fe–Co–O/Co@NC-mNS/NF) after *in situ* electrochemical oxidation of Co species (Fig. 10b–e). The XPS analysis discloses that the presence of $Fe^{3+}$ greatly activates the CoOOH species generated through *in situ* oxidation and exhibited a high performance towards the OER with 257 mV as the overpotential (Fig. 10f).[77] Instantly, Hao *et al.* fabricated a hierarchical architecture of Ni/C nanosheets by *in situ* growth on Ni foam (NF@Ni/C). In this study, they directly grew Ni-MOFs over the NF with prior oxidation, followed by calcination for 2 h at different temperatures (400–700 °C). The optimized catalyst NF@Ni/C-600 showed the best catalytic activity with a lower overpotential of 265 mV to reach a 50 mA $cm^{-2}$ current density. The higher catalytic activity of the OER is due to the encapsulation of Ni nanoparticles in an oxide shell over the graphitic carbon as evident from the *ex situ* XRD and XPS analysis.[78] Moreover, 3D (dimensional) N-doped carbon nanotubes derived from Co-MOF over the NF (Co-NCNTFs//NF) were developed by Yuan and his co-workers *via* solvothermal treatment followed by pyrolyzing at 600 °C with dicyandiamide (DCDA) powder. Like in the above discussion, the presence of metallic nanoparticles which are encapsulated/embedded in the shells of carbon will manifest the electronic interaction of CNTs. But this work explains that the use of DCDA will serve as an N-source, which will further induce the electronic modification between the metal nanoparticles and CNTs, thus providing more active sites for the facile OER process.[79] Han *et al.* developed a bimetallic NiCo-MOF derived porous microrod array ($NiCo@NiCoO_2$/C PMRAs) as a core@shell through a

 

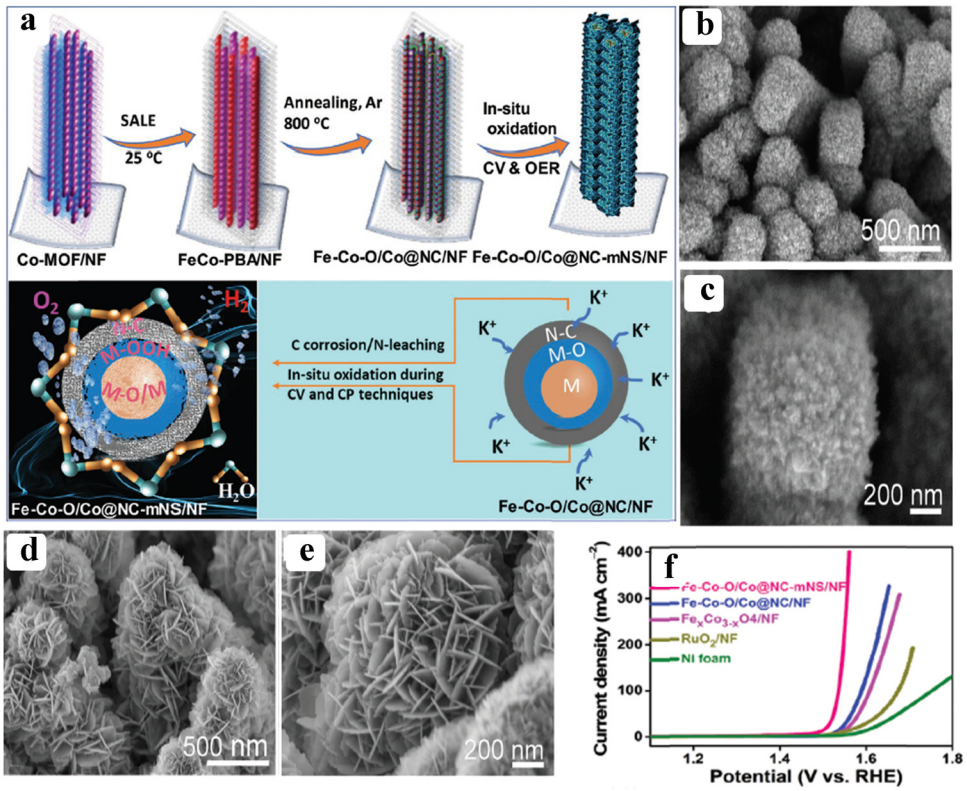


Fig. 10 (a) Schematic diagram denoting the *in situ* electrochemical transformation of Fe–Co–O/Co@NC to the *in situ* oxidized mesoporous nanosheet (mNS) structures on the NF with the possible mechanism; (b and c) and (d and e) show the FE-SEM images of Fe–Co–O/Co@NC/NF and *in situ* oxidized Fe–Co–O/Co@NC-mNS/NF; (f) corresponding LSV polarization results of Fe–Co–O/Co@NC-mNS/NF, Fe–Co–O/Co@NC/NF, $Fe_xCo_{3-x}O_4$/NF with $RuO_2$/NF and bare Ni foam. Reprinted with permission from ref. 77. Copyright (2021) Wiley-VCH.

reductive carbonization followed by subsequent oxidative calcination. Subsequently, the authors found that the presence of oxygen vacancies literally hikes the conductivity of $NiCoO_2$ and also enhances the charge transfer kinetics for the effective OER in alkaline solution. The optimized NiCo@$NiCoO_2$/C PMRAs requires a lower overpotential of 366 mV at 20 mA $cm^{-2}$ current density.[80] An interesting work by Lianzhou and co-workers reported a unique interfacial interaction between the Ni-MOF and graphene creating a freestanding 3D CNT/reduced graphene oxide (rGO) heterostructure film (Ni@N-HCGHF). According to this strategy, the CGHF is created by integrating 2D rGO sheets with a Ni-MOF-derived CNT microsphere superstructure with high surface area, porosity, controlled dopants, defect structure and enhancement in the conductivity. These factors influence the electron transfer pathway between the electrode/electrolyte ions, resulting in high performance of the OER. Fig. 11a illustrates the controllable synthetic process of Ni@N-HCGHF. The SEM and TEM results confirm the hollow microspheric nature of the Ni-MOF-derived N-doped carbon nanotubes (Fig. 11b). Also, high resolution TEM (Fig. 11c–e) further evidences the encapsulation of Ni nanoparticles responsible for the higher catalytic activity to the N-doped carbon nanotube. The XANES and EXAFS analyses showed peaks around 2.11 Å corresponding to the coordination of Ni–Ni, confirming the metallic state of Ni ($Ni^0$) in Ni@N-HCGHF and assuring the formation of Ni NPs (Fig. 11f and g). Furthermore, the EXAFS fitting (Fig. 11h) shows an *R*-factor value at 1.92 Å, corresponding to coordination of 3 N atoms with Ni in Ni@N-HCGHF. The free energy calculations from the DFT study also evidence the higher activity of Ni@N-HCGHF with an overpotential of 260 mV to reach 10 mA $cm^{-2}$ (Fig. 11i and j). Hence, the presence of N atoms in Ni@N-HCGHF further leads to partial adjustment of the electronic structure, creation of defective sites and further enhancement in conductivity, resulting in higher activity of the OER.[81] The above studies have motivated researchers to fabricate MOF derived carbon composites with various morphologies and functionalities.

## Metal nitrides/phosphides/sulfides/selenides derived from MOFs

MOFs can also be employed as a template for the synthesis of complicated nanostructured metal sulphides, selenides, nitrides and phosphides. Most of the first-row transition metals are developed as nanostructured metal sulphides, selenides, nitrides and phosphides as high performance electrocatalysts for water splitting reaction.[82–85] Regarding the OER, the catalytic cycle often involves the nucleophilic attack of reagents ($H_2O$ or $OH^-$) towards the high-valent metal-oxo intermediates.

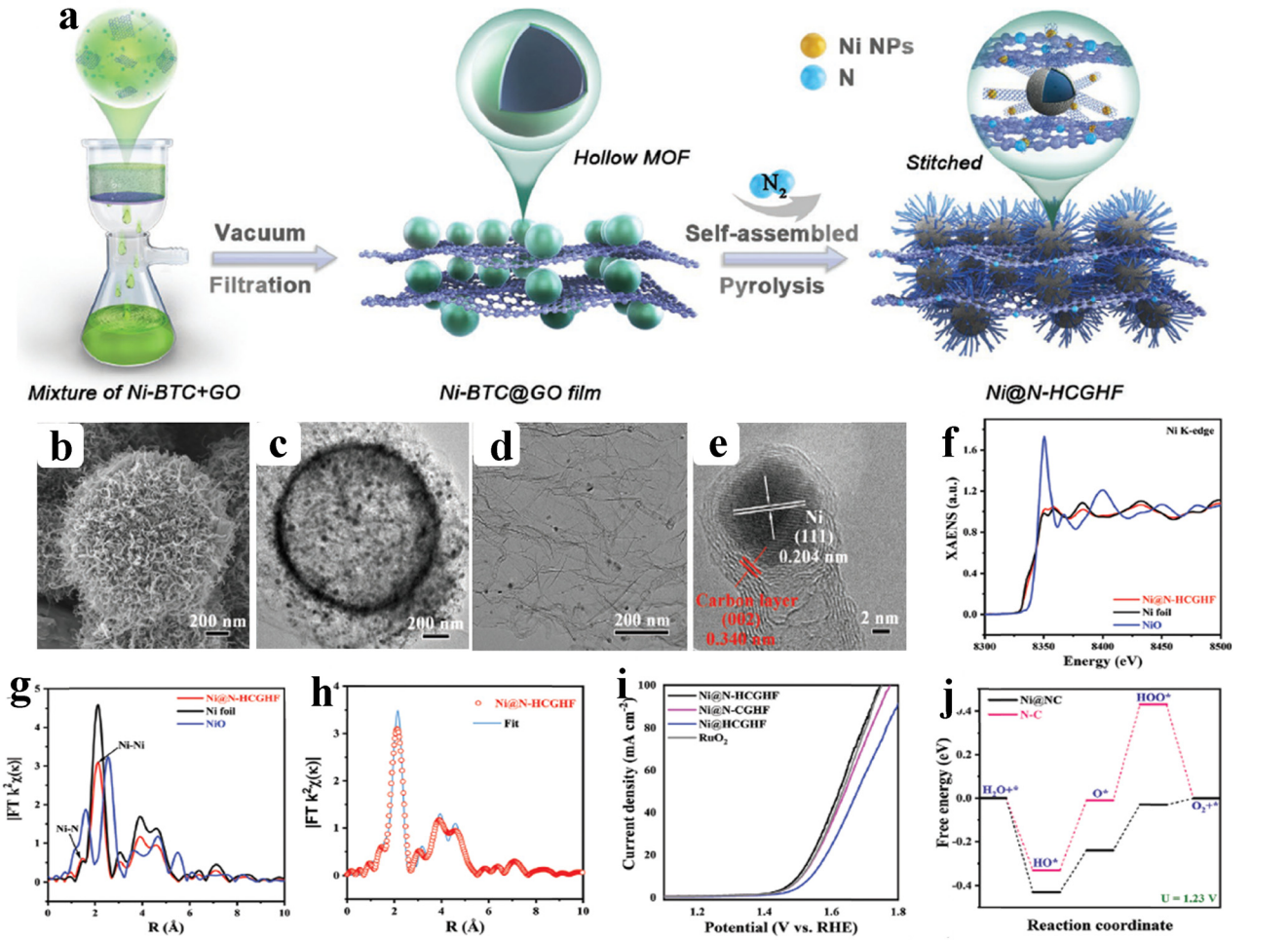


Fig. 11 (a) Schematic representation of Ni@N-HCGHF; (b) SEM and TEM images of N-doped MOF-derived carbon nanotube hollow microspheres; (b) FE-SEM images; (c–e) HR-TEM images of Ni@N-HCGHF; (f and g) Ni-K edge XANES spectra and FT-EXAFS of Ni@N-HCGHF, Ni foil, and NiO; (h) EXAFS fitting curves of Ni@N-HCGHF; (i) LSV outcomes of Ni@N-HCGHF, Ni@N-CGHF, Ni@HCGHF and $RuO_2$; (j) calculated Gibbs free energy diagram of the OER intermediates of Ni@N-HCGHF. Reprinted with permission from ref. 81. Copyright (2020) Wiley-VCH.

Due to strong electronegativity of the above heteroatoms attached to the metal centres, it is anticipated that the repulsion between the heteroatom's 3p orbital and oxygen's 2p orbital will prevent adhering of $OH^-$ ions. Nevertheless, the production of OOH* from OH* may be aided by the delocalization of electrons from the adsorbed oxygen, metal centres, and electronegative heteroatoms. Therefore, the repulsion of the 3p-2p site speeds up the oxidation of the OOH* intermediate.[76,86] Therefore, MOF derived metal sulphides, selenides, nitrides and phosphides will be another potential approach for delivering exceptional OER activity.

## MOF-derived metal selenides

In recent decades, selenide-based catalysts have been considered as a potential candidate for the OER process, because of the perfect electronic band structure and easily accessible valence and conduction edges.[11] According to Jahangir *et al.* the higher covalent percentage of M–X bond promotes the water oxidation reaction at the transition metal site, which is properly aligned at the valence and conduction band sites.[87] As previously stated, the electrocatalyst for the OER is preferred to have near-unity occupancy in the $e_g$ orbital of the transition metal cation. For example, Chundong *et al.* developed a conductive (Co,Ni)$Se_2$@NiFe LDH with the 3d orbital of Co possessing low spin $t^6_{2g}$ $e^1_g$ configuration with near unity for an effective OER process. In this work, they hierarchically developed a (Co,Ni)$Se_2$@NiFe LDH as hollow nanocages derived from the ZIF-67 precursor. Furthermore, they proposed a Ni–O–Co–O–Fe–O–Ni model to understand the synergism between the Ni, Co and Fe ions at the interface. This model displays that through the O-bridge, the electrons are transferred from $Ni^{2+}$ to $Co^{2+}$ and also simultaneously transfer to low spin $Fe^{3+}$ sites. This redistribution of electrons among the metal sites will increase the electrocatalytic activity of (Co,Ni)$Se_2$@NiFe LDH compared to the pristine materials.[88] Another study by Fang and co-workers reported a heterostructured bimetallic $CoSe_2$/ZnSe derived from the CoZn-MOF precursor as an electrocatalyst for the oxidation of water. It is suggested that higher activity is due to the effective electronic alignment as well as

 

a phase-boundary effect between hexagonal ZnSe and cubic $CoSe_2$ (Fig. 12a–e). The use of a MOF precursor will facilitate the optimal interface between the two phases obtained from the transformation. Also, the electron transfer from the $CoSe_2$ to ZnSe *via* the interface leads to redistribution of electrons over the metal sites, which helps the adsorption of $OH^-$ ions (Fig. 12f). Furthermore, EXAFS analysis implies that higher activity is due to the Jahn–Teller distortion in $CoSe_2$ ($Co^{2+}$, $t^6_{2g}$ $e^1_g$) and heterogeneous spin states coexist in the phase boundary, but there is no Jahn–Teller distortion in ZnSe ($Zn^{2+}$, $3d^{10}$). Hence, the higher activity is obtained from the extended phase boundary and the lattice distortion of bimetallic CoZn-selenides.[89] Another study also by Wenjiao *et al.* reported bimetallic MOF-derived hollow $(Ni,Co)Se_2$ arrays over CC as an efficient electrocatalyst for the OER. Firstly, triangle-like MOFs are grown over the CC, and then incorporation of Ni was done by ion exchange and etching in the presence of $Ni(NO_3)_2$. Then the formed intermediate is subjected to selenization through a solvothermal treatment at 140 °C for 10 h. The resulting $(Ni,Co)Se_2$ electrode demonstrates good electrochemical activity and stability by making use of the structural, compositional, and self-supporting characteristics. The selenized NiCo exhibits a low onset overpotential of 226 mV to reach a benchmarking current density. Due to the hollow nature of $NiCoSe_2$, the reagent $OH^-$ will easily interact with active sites present inside the hollow structure.[90] A multiphase bimetallic NiFe selenide derived from NiFe PBAs as MOF precursors over carbon fiber paper (NiFe-Se/CFP) as an efficient electrocatalyst for water oxidation reaction was reported by Guo and co-workers. They followed a two-step electrodeposition for the synthesis of NiFe-PBAs over the CC, followed by subsequent selenization *via* post-thermal pyrolysis at 450 °C for 30 min (Fig. 12g). The resultant selenized NiFe over the CC displays two mixed phases of $NiSe_2$ and $Fe_2NiSe_4$ structures. The $Fe_2NiSe_4$ phase possesses higher catalytic activity with a low onset overpotential of 281 mV (Fig. 12h) in 1 M KOH solution. The XPS

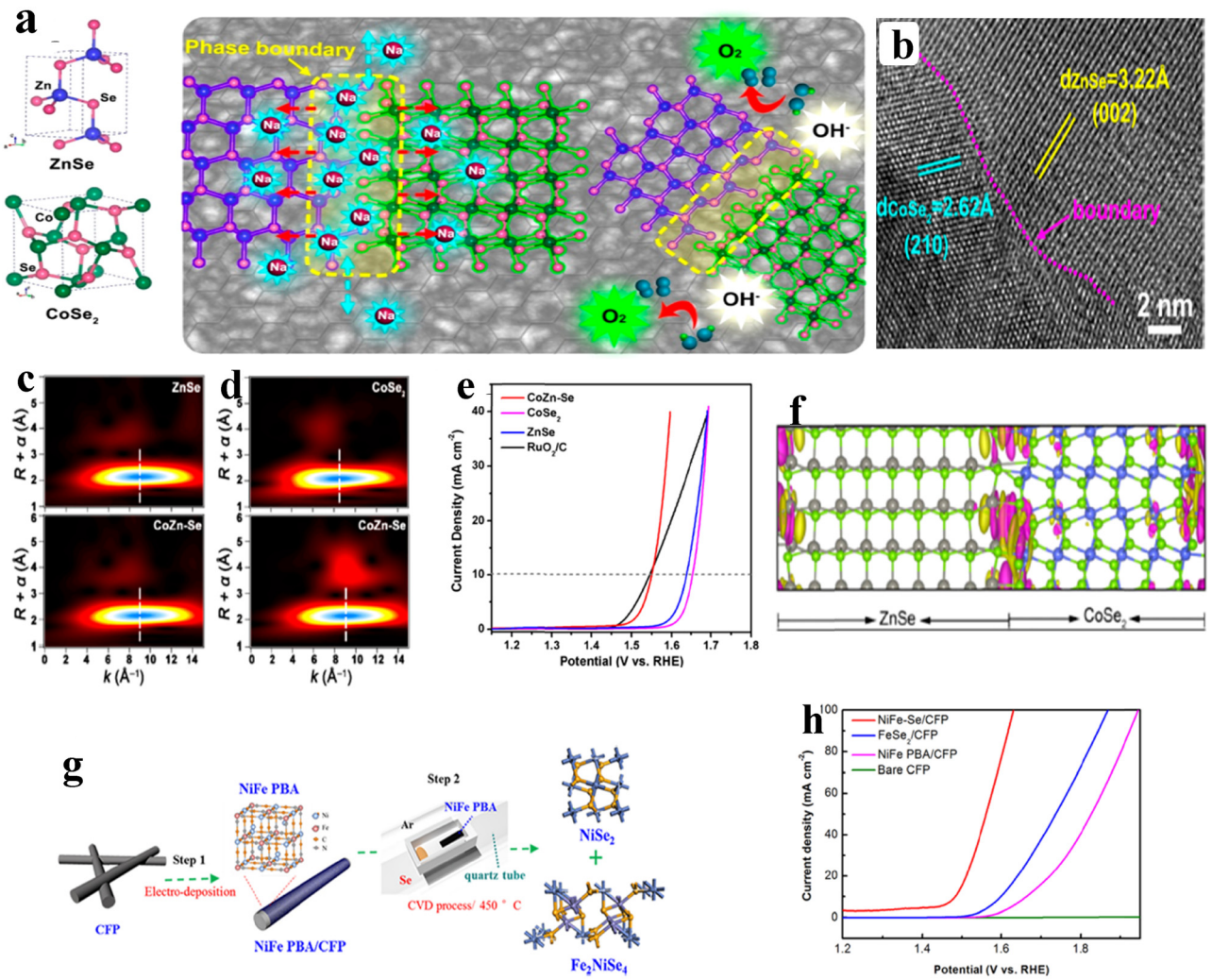


Fig. 12 (a) Schematic diagram of the phase boundary effect in CoZn–Se; (b) HR-TEM image showing the boundary between CoSe and ZnSe; (c and d) $k_2$-weighted K-edge EXAFS signals of Zn and Co for ZnSe and CoZn-Se, respectively; (e) LSV curves of CoZn-Se, CoSe, ZnSe and $RuO_2$; (f) charge density profile at the phase boundary between CoSe and ZnSe; (g) schematic illustration of NiFe-Se/CFP synthesis; (h) LSV polarization results of NiFe–Se, $FeSe_2$ and NiFe PBA over CFP. Reprinted with permission from ref. 90. Copyright (2021) American Chemical Society (ACS).

analysis results in the formation of γ-NiOOH phase in the NiFeSe, a significant active phase for the high performance of the OER.[91]

## MOF-derived metal sulfides

The MOF-derived transition metal-based sulfides have also garnered considerable interest due to their similar physicochemical characteristics to selenides. In recent years, numerous studies have been reported on adjusting the stoichiometry of sulfides to enhance their capabilities in water splitting. However, there is a lot of room for improvement in the catalytic activity by manipulating the morphology, structure, and composition of these materials.[2,92] Li and his colleagues developed *in situ* grown $[Ni_3(OH)_2(1,4\text{-BDC})_2\text{-}(H_2O)_4]\cdot 2H_2O$ 2D nanosheet arrays on NF, followed by decoration of sulfide *via* partial sulfurization treatment in presence of thioacetamide. A hierarchical framework that was created *in situ* may support mass transit and also strengthen the structural integrity, resulting in effective and consistent OER performance.[93] Similarly, another group introduced $Fe^{3+}$ ions into the Ni-MOFs to prepare ultrathin nanosheet of NiFe-MOFs over NF, as seen in Fig. 13a. Like the previous discussion, partial sulfurization treatment was employed to obtain a NiFe-MS/MOF@NF. The XRD spectrum confirms the formation of the MIL-53 type MOF and $Ni_3S_2$ with a heazlewoodite-structure. The enhancement in OER activity is attributed to the infused sulfides in the ultrathin nanosheets, which greatly increase the surface area and conductivity. In addition, the electronic structure is modified to an electron rich site, which facilitates the adsorption of oxygen intermediates.

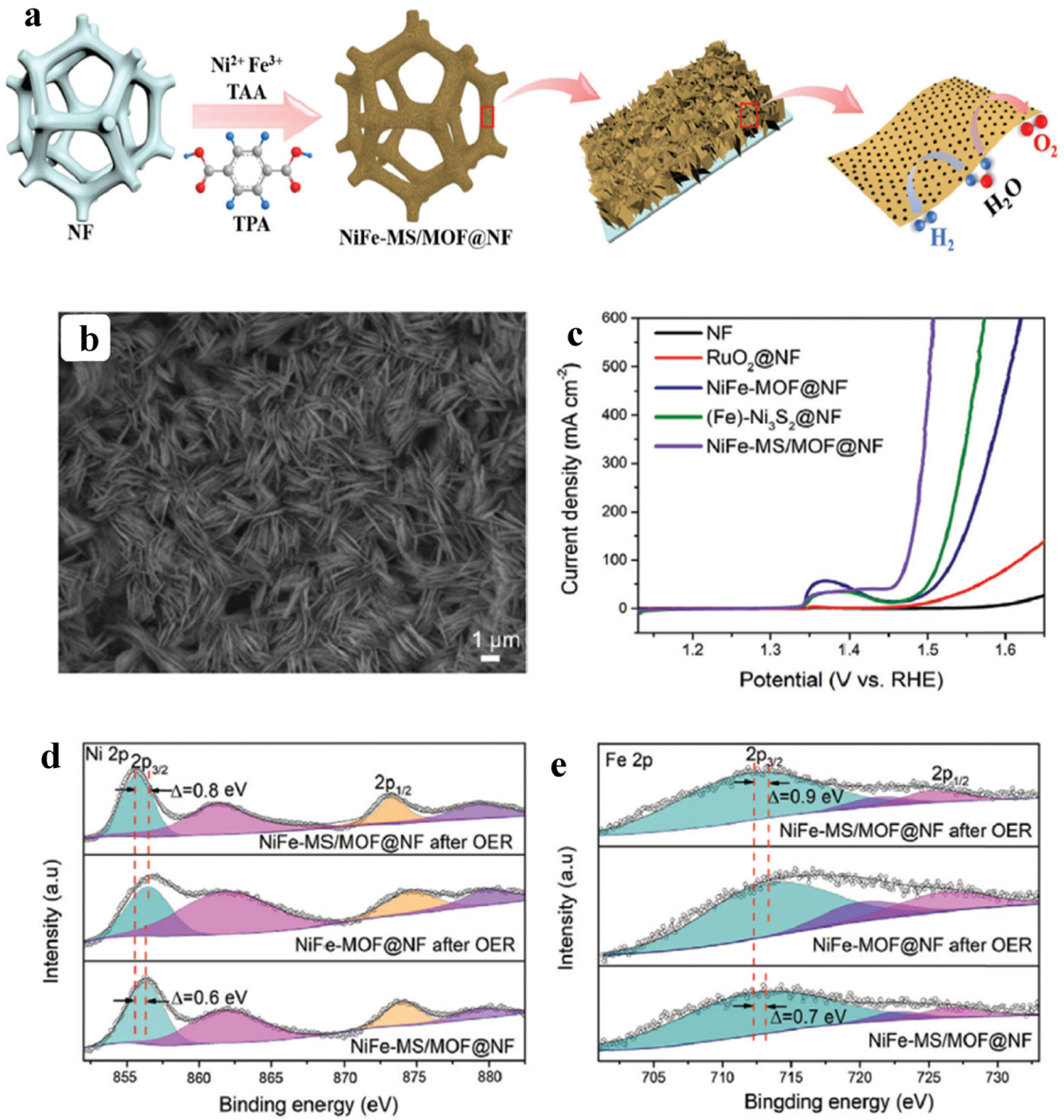


Fig. 13 (a) Schematic illustration of NiFe-MS/MOF@NF synthesis; (b) SEM images of NiFe-MS/MOF@NF; (c) corresponding LSV polarization results; (d and e) XPS analysis of Ni and Fe 2p orbitals of NiFe-MS/MOF@NF. Reprinted with permission from ref. 94. Copyright (2020) Wiley-VCH.

 

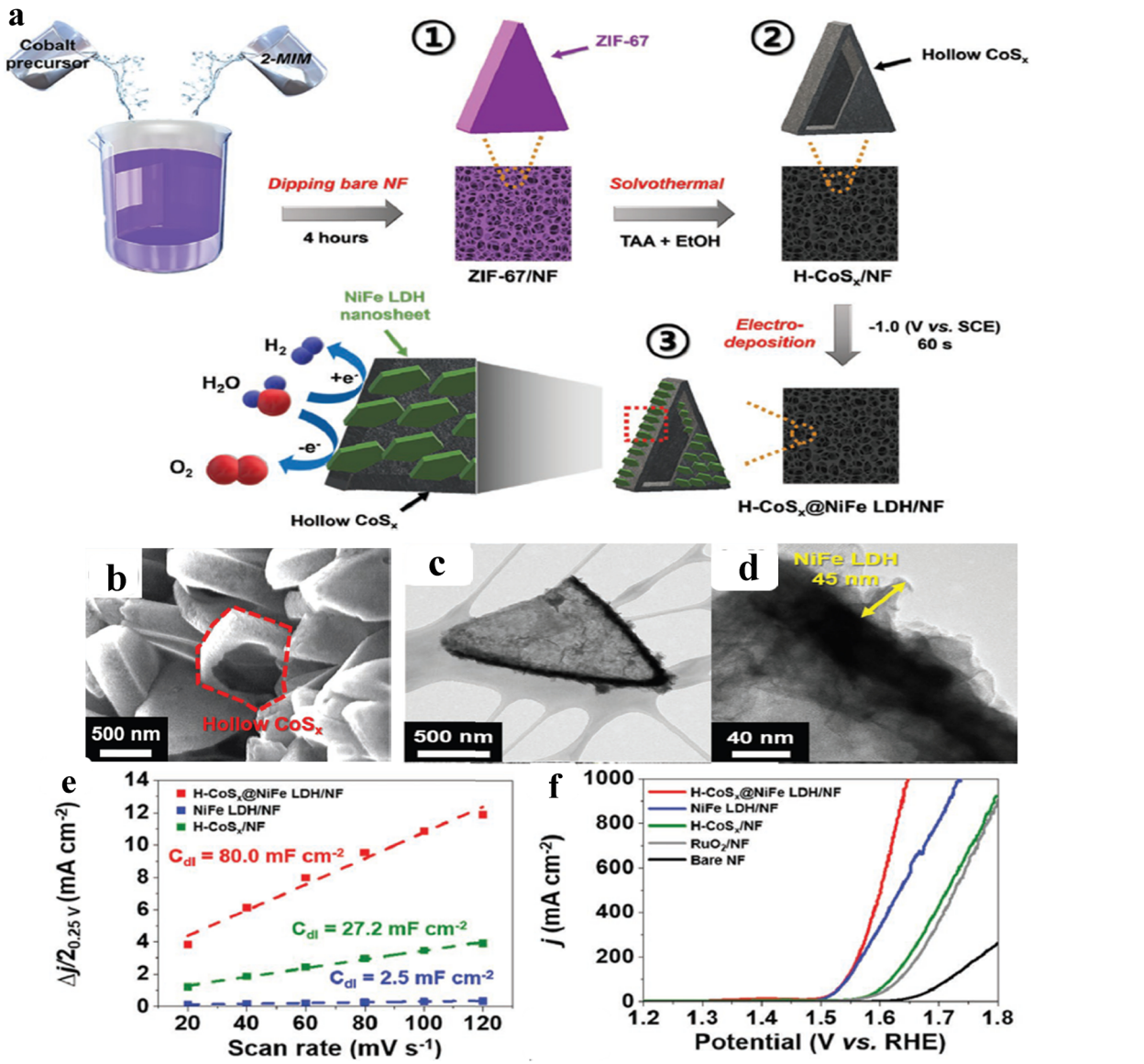


Fig. 14 (a) Schematic diagram of the fabrication process of H-$CoS_x$@NiFe LDH/NF; (b) SEM images of H-$CoS_x$/NF; (c and d) TEM and HR-TEM images of H-$CoS_x$/NF; (e) calculated $C_{dl}$ values at current densities *vs.* scan rates; (f) OER performance of all the catalysts at 1 M KOH solution. Reprinted with permission from ref. 96. Copyright (2022) Wiley-VCH.

The higher activity and modulation of the electronic structure of NiFe-MS/MOF@NF was evident from the FE-SEM and XPS analysis seen in Fig. 13b–e.[94] In another example, by employing $SO_4^{2-}$ as an S source, Renzhi *et al.* prepared Ni–$Ni_3S_2$@carbon nanoplates under Ar atm. The 2D Ni-MOF nanoplates were fabricated by coordination between 4,4′-bipyridine and $NiSO_4$ with pyridine as a freestanding precursor for N-doped Ni–$Ni_3S_2$@carbon nanoplates. The added pyridine effectively inhibits the thickness of the unique core–shell structure, which is responsible for the higher OER performance.[95] Recent reports on coupling OER and HER active materials are considered as a rational strategy for high performance OER electrocatalysts. For instance, through a simple solvothermal reaction with thioacetamide as an S source, Yun *et al.* transformed solid ZIF-67 nanoarrays into hollow $CoS_x$ (H-$CoS_x$) nanoarrays, as seen in Fig. 14a. By adopting electrodeposition method, they deposited a NiFe-LDH nanosheet hierarchically over the nanoarrays of $CoS_x$ to form hollow structured nanoarrays (H-$CoS_x$@NiFe LDH). The TEM and SEM images in Fig. 14b–d clearly display the lamellar NiFe-LDH and hollow structure of H-$CoS_x$@NiFe LDH. The presence of lamellar NiFe-LDH enhances the specific active surface sites, evident from the double layered capacitance ($C_{dl}$) of H-$CoS_x$@NiFe LDH from Fig. 14e. As a result, the existence of more surface-active site leads to lesser overpotential of 250 mV at 10 mA $cm^{-2}$ current density (Fig. 14f).[96]

## MOF-derived metal phosphides

Metal phosphides have evolved as a novel class of improved catalysts for electrochemical water splitting. Despite the high

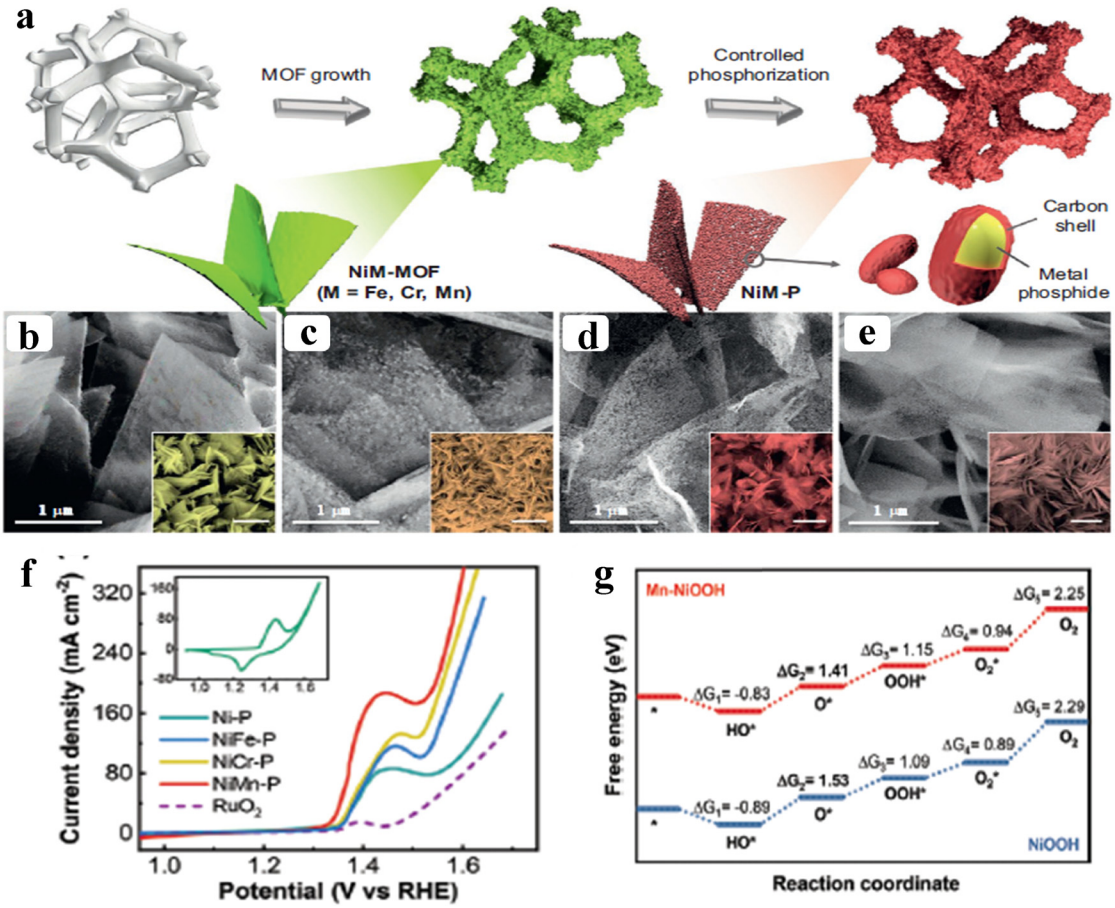


Fig. 15 (a) Schematic representation of the synthetic process of NiM–P (M = Fe, Cr, Mn); (b–e) corresponding SEM images of Ni–P, NiFe–P, NiCr–P and NiMn–P, respectively; (f) LSV results of the OER in 1 M KOH medium; (g) optimized free energy diagram of NiMn–P and undoped Ni–P towards the OER. Reprinted with permission from ref. 99. Copyright (2021) Wiley-VCH.

performance of metal phosphides, the performance of monometallic phosphides is still constrained. So, incorporation, doping or creating a heterointerface between metal and metal phosphide components is a fruitful strategy to enhance the electrochemical activity. For instance, 1D interfaced $Co_3O_4$/$Fe_{0.33}Co_{0.66}P$ nanowires were fabricated by Xiaoyan *et al. via* partial chemical etching of $Co(CO_3)_{0.5}(OH)_{0.11}H_2O$ (Co-CHH) with $[Fe(CN)6]^{3-}$ followed by phosphorization treatment. The studied interface (IF) model evidenced that the interface is rich in electron–holes suggesting the empty state of the LUMO near the Fermi level. The d-band centre study shows the downshifts in the d-orbital of the Co-3d band and the intermediate Fe-3d band will simultaneously regulate the electronic structure. The P-3p band near the Fermi level will reduce the binding ability among P and O sites and facilitate the OER. The resulting nanowired interface $Co_3O_4$/$Fe_{0.33}Co_{0.66}P$ exhibits a very high activity with a low overpotential of 215 mV to get a 50 mA $cm^{-2}$ current density with long-term static stability for 150 h.[97] Furthermore, to enhance the material stability and performance, doping of noble metals like Ru will be a promising strategy. For example, Chen *et al.* constructed a bimetallic 3D flower like NiCoP with Ru doping over the conductive NF derived from the Co-ZIF. This yields a better electrocatalytic activity towards the OER with an overpotential of 216 mV at 20 mA $cm^{-2}$ current density in 1 M KOH solution. As a result, the introduction of Ru enhances the higher electron kinetics, the morphology offers easy accessing of more active sites by electrolyte solution and the cohesive force between the *in situ* grown catalyst and the substrate.[98] Moreover, Lin and co-workers designed a hierarchically grown spongy nanosheet over NF composed of carbon encapsulated $Ni_2P$ nanoparticles followed by controlled phosphorization, as seen in Fig. 15a. The series of metal doping, like Fe, Cr and Mn, made the Ni–P nanosheets into a more clear nano-spongy structure evident from Fig. 15b–e. Upon insertion of secondary metal ions, in addition to morphology change, electronic structure also modulated the results in the adsorption strength of the $OH^-$ and their intermediate ions. Among the doped metal ions, Mn doped Ni–P provided better catalytic activity than the Fe, Cr doped Ni–P with a low overpotential of 190 and 245 mV at 10 and 50 mA $cm^{-2}$ current density, respectively. The adsorption Gibbs free energy profile from the DFT analysis evident from Fig. 15f and g suggested that Mn-doped Ni–P possesses a lower adsorption energy of 1.41 eV for the conversion of OH* to O*.[99] Moreover, trimetallic

 

MOF-derived phosphides also provide a prominent active site for adsorption of $OH^-$ ions. For example, Ghising *et al.* prepared a trimetallic Ni–Fe–Mn–P, co-doped with N and C grown *in situ* on NF for efficient OER. The N and C are encapsulated with the hybrid carbon shell derived from the trimetallic MOF ultrathin nanosheet. The co-doped N,C trimetallic Ni–Fe–Mn–P (Ni–Fe–Mn–P/NC@NF) demands a low overpotential of 274 mV at 30 mA $cm^{-2}$ current density with 56.8 mV $dec^{-1}$ as the Tafel slope value and suggesting faster electron kinetics than the pristine materials. Besides, the porous nature and large specific area, presence of unsaturated active metal ions and electron rich N and P facilitate the adsorption of reagents for the OER.[100]

## MOF-derived metal nitrides

Among the metal derivatives like sulfides, selenides, phosphides and nitrides, the later one is gaining more attention in recent times possibly due to exceptional electronic structures, high electrical conductivity and long-term durability in a wide range of pHs. In particular, the d-band density of the metal atoms is altered by the negatively charged nitrogen atoms which will be helpful for the catalytic applications.[101] According to the literature, compared to monometallic nitrides, bimetallic nitrides will enhance the electrocatalytic performance by reducing the kinetic energy barrier. The electronic structure and electron density of the bimetallic material can be efficiently changed by the addition of a second metal, which will enhance the free energy of reagent adsorption. For example, Fu's research group designed a hollow Co–$Mo_2N$ hybrid through a 'MOF plus MOF' strategy. In this approach, 1 D Mo-MOFs were first grown like a rod and using ZIF-67, Co-MOFs were fabricated over the rod like 1D Mo-MOFs and the resultant MoCo-MOFs were converted to the corresponding nitride *via* pyrolysis under an $NH_3$ environment. The combination of two MOFs will provide a flexible synergistic contact between the inner $Mo_2N$ and outer Co layer leading to a synergistic increase in OER performance with an overpotential of 302 mV (without *iR* correction) to meet 10 mA $cm^{-2}$.[102] Recently, the introduction of carbonaceous materials towards transition metal nitrides will greatly increase the performance of water splitting. For instance, Yoon and co-workers developed a mesoporous $Co_3N$/amorphous N-doped carbon nanocube (ANC-NCs) which is grown *in situ* over the 3D NF derived from the Prussian blue analogue (PBA) and followed by a subsequent nitridation/calcination process, as seen from Fig. 16a. The resultant catalyst exhibited a high performance towards the OER with an overpotential of 280 mV at 10 mA $cm^{-2}$ current density as shown in Fig. 16f. The high performance of the optimized $Co_3N$@AN-C is due to the presence of a large specific surface area provided by the distinctive mesoporous structure with attached particles, influenced by the *in situ* growth of an AN-C over $Co_3N$ nanoparticles as observed in FE-SEM and

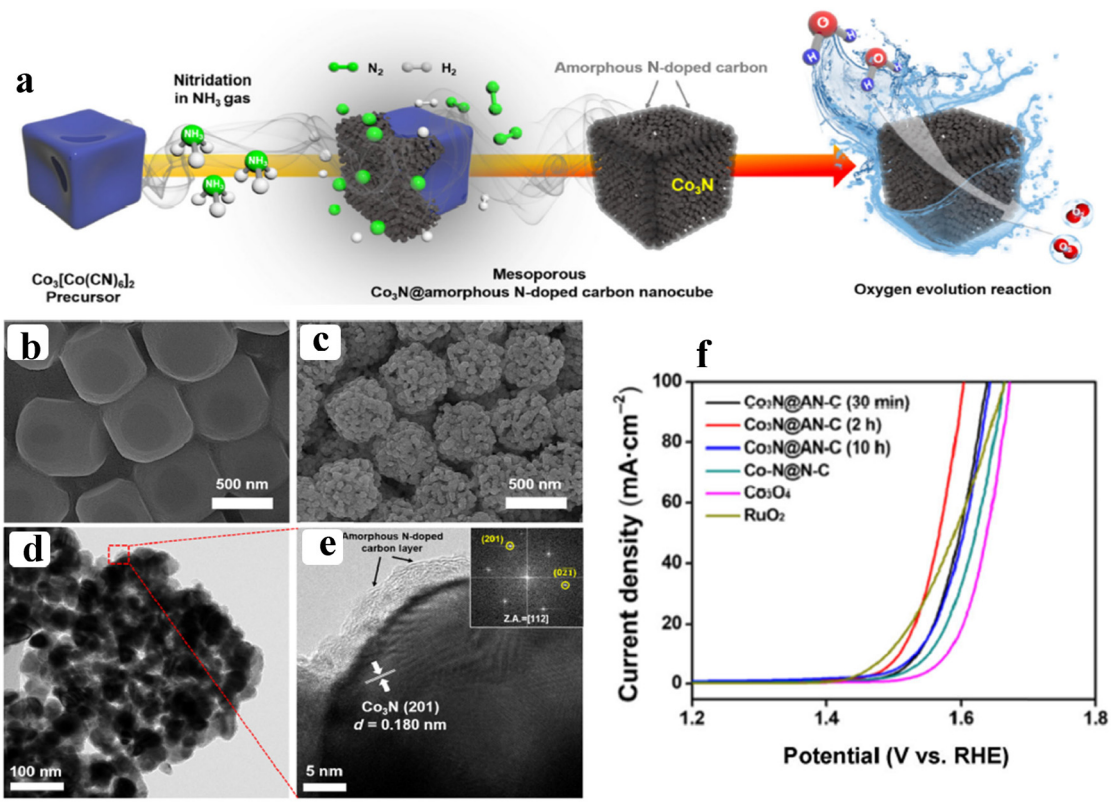


Fig. 16 (a) Schematic illustration of $Co_3N$@amorphours N-doped carbon NCs employed for the OER; (b and c) FESEM images of $Co_3[Co(CN)_6]_2$ PBA and $Co_3N$@AN-C NCs; (d and e) TEM and HR-TEM images of $Co_3N$@AN-C NCs (inset image is FFT patterns); (f) IR corrected LSV polarization curves of $Co_3N$@AN-C NCs, Co-N@N-C, and $Co_3O_4$ NCs. Reprinted with permission from ref. 103. Copyright (2019) Springer.

Table 2 A comparison of the OER performance of MOF-derived nanostructures as electrocatalysts

| S. No. | Electrocatalyst | Substrate | Overpotential (mV) | Current density | Tafel slope (mV $dec^{-1}$) | Electrolyte | Ref. |
|---|---|---|---|---|---|---|---|
| 1 | (Ru–Co)$O_x$-350 | GCE | 265 | 10 mA $cm^{-2}$ | 60 | 1 M KOH | 69 |
| 2 | Ru-NiFe-MOF | NF | 310 | 100 mA $cm^{-2}$ | 42.7 | 1 M KOH | 70 |
| 3 | ZnCo–Fe-20 | GCE | 176 | 10 mA $cm^{-2}$ | 69.3 | 1 M KOH | 71 |
| 4 | $Co_3O_4$/Co–Fe oxide DSNBs | GCE | 297 | 10 mA $cm^{-2}$ | 61 | 1 M KOH | 72 |
| 5 | NiCo/$Fe_3O_4$/MOF-74 | GCE | 238 | 10 mA $cm^{-2}$ | 29 | 1 M KOH | 73 |
| 6 | (Ru–Co)$O_x$ | CC | 171 | 10 mA $cm^{-2}$ | 60 | 1 M KOH | 74 |
| 7 | Co-$RuO_2$ | CC | 238 | 10 mA $cm^{-2}$ | 48 | 1 M KOH | 75 |
| 8 | Fe–Co–O/Co@NC-mNS | NF | 257 | 10 mA $cm^{-2}$ | 41.5 | 1 M KOH | 77 |
| 9 | NF@Ni/C-600 | NF | 265 | 10 mA $cm^{-2}$ | 54 | 1 M KOH | 78 |
| 10 | Ni@N-HCGHF | GCE | 260 | 10 mA $cm^{-2}$ | 63 | 1 M KOH | 81 |
| 11 | (Co,Ni)$Se_2$@NiFe LDH | GCE | 277 | 10 mA $cm^{-2}$ | 75 | 1 M KOH | 88 |
| 12 | $CoSe_2$/ZnSe | GCE | 320 | 10 mA $cm^{-2}$ | 66 | 1 M KOH | 89 |
| 13 | NiFe-Se | CFP | 281 | 10 mA $cm^{-2}$ | 40.9 | 1 M KOH | 91 |
| 14 | Ni-BDC@NiS | NF | 330 | 20 mA $cm^{-2}$ | 62 | 1 M KOH | 93 |
| 15 | NiFe-MS/MOF | NF | 230 | 50 mA $cm^{-2}$ | 32 | 1 M KOH | 94 |
| 16 | H-$CoS_x$@NiFe LDH | NF | 250 | 10 mA $cm^{-2}$ | 49 | 1 M KOH | 96 |
| 17 | Ru-NiCoP | NF | 216 | 20 mA $cm^{-2}$ | 84.5 | 1 M KOH | 98 |
| 18 | NiMn-P | NF | 190 | 10 mA $cm^{-2}$ | 38 | 1 M KOH | 99 |
| 19 | Co–$Mo_2N$ | RDE | 346 | 10 mA $cm^{-2}$ | 90 | 1 M KOH | 102 |
| 20 | Co3N@AN-C NCs (2 h) | CP | 280 | 10 mA $cm^{-2}$ | 69.6 | 1 M KOH | 103 |
| 21 | CoNi(1:1)-MOF | Copper foils | 265 | 10 mA $cm^{-2}$ | 56 | 1 M KOH | 105 |

GCE-glassy carbon electrode; CFP-carbon fiber paper; NF-nickel foam; CC-carbon cloth; RDE-rotating disk electrode; CP-carbon paper.

HR-TEM images from Fig. 16b–e.[103] On the other hand, Zhang *et al.* adopted an interfacial scaffolding strategy, to construct hierarchical CoFe-PBA@$Co(OH)_2$/NF cubic nanosheets, later transformed into the respective nitride *via* pyrolysis under an $NH_3$ atmosphere. After pyrolysis the nanosheets are well-retained, which significantly increases the OER performance with an overpotential of 270 mV to reach a current density of 20 mA $cm^{-2}$ and exhibits an outstanding durability for 1200 h. This versatile approach offers a methodology for the logical design of PBA-based functional nanomaterials, which holds great promise in electrocatalytic applications.[104] In another work by Liu *et al.*, the 2D CoNi-MOF as a nanoplate was developed over a copper foam (CF) substrate. With further annealing under an $NH_3$ atmosphere, the pristine CoNi-MOF is converted to CoNiN nanoplate arrays on an amorphous carbon network. This metallic nitride array on an amorphous carbon network yields a higher activity with an overpotential of 265 mV at 10 mA $cm^{-2}$ in alkaline medium.[105] In summary, a comparison table of OER performance for MOF derived nanostructures as electrocatalysts is provided in Table 2.

## Effect of the morphology of MOF-based materials towards OER performance

Generally it is well known that, apart from chemical composition, morphology and micro-sized electrocatalysts play a crucial role in their physico-chemical properties. The logical engineering and designing of the morphology dependent intricate nanostructures with a large specific surface area are required in order to achieve significant catalytic activity. As a result, MOF-based electrocatalysts with tuneable morphologies will induce disparate exposed active sites, which boosts the adsorption of active reagents ($H_2O/OH^-$) during the OER process. For instance, Qichun *et al.* developed a series of morphology-regulated (nanosheets, nanoflowers, nanotubes and aggregations) Hofmann-type FeNi-MOFs by simply tuning the amount of PVP at room temperature as an effective electrocatalyst for efficient OER in an alkaline medium. It was observed that among the different morphologies of FeNi-MOFs, MOFs possessing nanosheets showed a better electrocatalytic performance of 248 mV overpotential to attain a 10 mA $cm^{-2}$ current density. Fig. 17a shows the schematic illustration strategy of the morphology regulated FeNi-MOF derived electrocatalyst. The SEM images of the synthesised MOF precursors at different reaction conditions are provided in Fig. 17b–e. They obtained the various morphologies (Fig. 17f–i) of FeNi-MOF, possessing nanosheets (NSs), nanoflowers (NFs), nanotubes (NTs) and aggregations (AGs) after pyrolysis at high temperature and partial oxidation of the FeNi-MOF precursor. Interestingly, from the XPS analysis, they have found that the shifting of the binding energy towards a higher value in the case of Ni 2p and exists in the order of FeNi NFs, FeNi NTs and FeNi AGs than the FeNi NSs which implies that regulation of the morphology will also tune the electronic structure and the electrons will be transferred from the Ni site to the Fe site. The LSV polarization outcomes (Fig. 17j) evidence that FeNi NSs have better electrocatalytic activity than the FeNi NFs, FeNi NTs, FeNi AGs and commercial $RuO_2$ at 10 mA $cm^{-2}$, which are 248 mV, 258 mV, 284 mV, 332 mV and 286 mV, respectively. These results showed that by tailoring the morphology of FeNi-MOF, numerous exposed active sites and porous structures are created, which will boost the OER performance.[18] On the other hand, Yao *et al.* prepared a series of Fe-MOFs with polyhedral morphology by introducing $\beta$-cyclodextrin (CD) as a morphological modifier in the presence of ferric chloride and terephthalic acid (TPA) under dimethyl

 

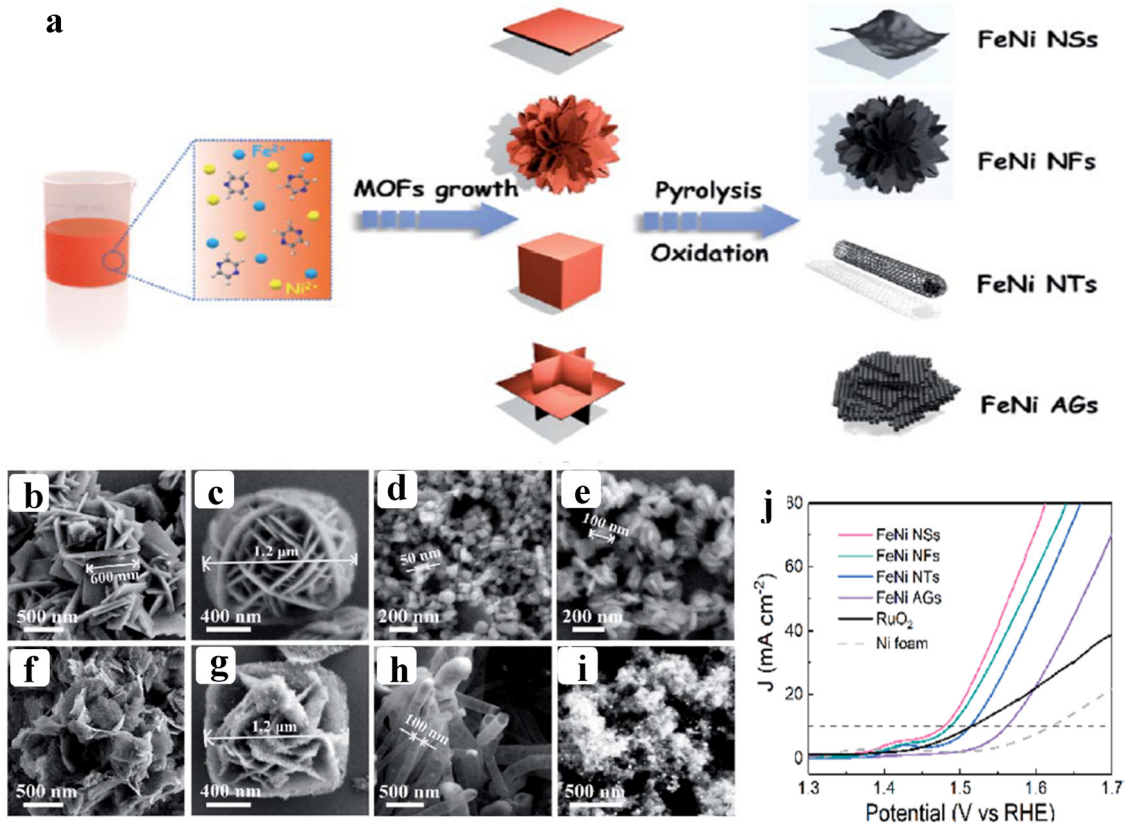


Fig. 17 (a) Schematic representation of various geometries of FeNi Hofmann MOF-derived electrocatalysts for the OER; (b–e) and (f–i) show the SEM images MOF precursors in different reaction systems and FeNi NSs, FeNi NFs, FeNi NTs and FeNi AGs, respectively; (j) LSV polarization results of FeNi-MOFs with various morphologies. Reprinted with permission from ref. 18. Copyright (2020) Royal Society Chemistry (RSC).

formamide (DMF) as a solvent. They regulated the morphology from a hexagonal bipyramid to a bipyramidal hexagonal prism by simply tuning the ratio of TPA to β-CD: 1 : 0, 1 : 1, 1 : 2, and 1 : 4 and observed a big difference in their structure. Among the optimized structures, Fe-MOF-1 shows high catalytic activity among all the structured Fe-MOFs with an overpotential of 398 mV to reach a 10 mA $cm^{-2}$ current density.[106] Recently, Jia *et al.* adopted a controllable synthesis of two-dimensional Fe–Ni MOF of $Fe(py)_2Ni(CN)_4$ (py = pyridine) yielding a variety of nanostructures, including nanoboxes, nanocubes, nanoplates, and nanosheets. Interestingly, Fe–Ni MOF nanoboxes deliver a high electrocatalytic activity with a 285 mV overpotential and a small Tafel slope value of 50.9 mV $dec^{-1}$ in a 1 M KOH solution.[107] In summary, tuning or engineering the morphology of the MOF-based electrocatalyst will provide a greater number of intrinsic exposed active sites, which might be due to the varied exposed crystal planes. These exposed active sites will further boost the electrocatalytic OER performance.

## Conclusion and future perspectives

The electrochemical process of water splitting is one of the most practical ways to generate hydrogen. So far numerous types of electrocatalysts have been scrutinized for electrochemical water-splitting. Among the several electrocatalysts, electrocatalysts made of MOFs have garnered a lot of attention. We have reviewed the most recent (as of 2018) developments in the field of OER electrocatalysis involving MOFs and their derivatives. Owing to their distinctive physicochemical characteristics, MOFs provide a number of benefits over traditional heterogeneous catalysts, including large surface area, well defined and highly versatile porous structures, easily tunable structures to get the desired morphology, and varied composition of MOF's to enhance the electrocatalytic OER performance. These advantages allowed for the successful fabrication of powder-based MOFs and integrated binder-free MOF electrodes with conductive substrates, which demonstrated good OER performance as a result of increase in conductivity. Additionally, MOFs can be used as templates to synthesize a variety of derivatives, including metal-derived carbons from MOFs, metal oxides, sulphides, selenides, phosphides and nitrides. These derivatives have a flawless MOF microstructure as well as the benefits of outstanding chemical and mechanical stability. The MOF derived electrocatalysts have several advantages, such as: by carefully tweaking the architectures and composites, it is simple to control the distribution of metal ions and doping atoms; MOF derivatives with highly porous and mesoporous structures provide a high electron transfer pathway towards the OER, improving the better contact between the different potential phases and electrical conductivity.

The current review has focused on the latest advancements in MOF's as sophisticated and effective electrocatalysts for the OER and various structural techniques to optimize their electrocatalytic activity. Even though MOF-based OER electrocatalysis has made significant strides, there are still some substantial problems and difficulties that need to be resolved before this field can provide effective materials for energy conversion.

(i) The first and foremost flaws of MOF electrocatalysts are conductivity for practical applications. Even while connecting MOFs with 3D conductive metal substrates has been shown to be a successful method for increasing conductivity, but it is not a universal technique for the majority of MOFs. Also, the preparation of ultrathin MOFs is a technique to enhance the electrical conductivity of the electrocatalyst. To address this issue, functionalization of MOFs with a conjugated organic linker or coupling carbon materials like carbon nanotubes, graphene and so on is used to enhance the inherent conductivity of the MOF based electrocatalyst.

(ii) Another drawback is the poor long-term static stability, which limits the large-scale viable application at harsh applied potential and also in corrosive electrolytic conditions. Novel designs and strategies are therefore required to increase the stable nature of MOFs. In addition, MOF-based electrocatalysts will be typically active in alkaline environments but not in acidic environments due to the easily available $OH^-$ ions leading to boost the reaction kinetics. As a result, it is currently challenging to create effective and stable MOFs for OER electrocatalysis in acidic and neutral media.

(iii) It is important to remember that the synthesis of MOFs occasionally needs an expensive organic ligand other than ZIF-67 and PBAs. So, it is necessary to explore the MOFs with popularization of other low-cost ligands as effective electrocatalyst *via* encapsulation of active metal atoms/nanoparticles to extend a variety of new functionalized MOFs towards the OER.

(iv) By appropriately controlling the crystal shape, it might be possible to directly use MOFs as OER electrocatalysts. It appears that ultrathin 2D MOF nanosheets are particularly well suited for water electrolysis.

(v) Upon proper surface functionalization, such as doping with heteroatoms, tuning of morphology, hydration of different components, and creation of oxygen vacancies and also selection of suitable composition of MOF's further extends the way towards other related electrocatalytic applications.

(vi) The reaction mechanism of the OER on MOFs is still not comprehended. So, it is imperative to employ the *operando* and *in situ* characterization techniques to determine the appropriated intermediates of the OER. Additionally, theoretical modelling and computational techniques are an effective tool for understanding the catalytic mechanisms.

Even though there are still many obstacles to overcome, the research on MOFs and their derivatives in the field of electrocatalysis, along with a deeper comprehension of the reaction mechanism, will provide a huge amount of information on the MOFs and their derivatives to help researchers to design better MOF-related electrocatalytic materials, ultimately leading to their widespread use in large scale generation of green hydrogen.

## Conflicts of interest

There are no conflicts to declare.

## Acknowledgements

Ragunath Madhu and N. Sreenivasan wish to acknowledge Department of Science and Technology (DST) for the Fellowship (SRF and JRF) respectively. Arun Karmakar, Krishnendu Bera, and N. D. Hariharan wish to acknowledge CSIR-HRDG for the SRF and JRF fellowship. Suprobhat Singha Roy wishes to acknowledge UGC for the JRF fellowship. Aditi De and S Kundu wish to acknowledge the Department of Science and Technology (DST) for CRG research funding with funding number # CRG/2021/001089 dated November 20th 2021 having CSIR-CECRI project number GAP 22/2021. CSIR-CECRI Manuscript number: CECRI/PESVC/Pubs/2023-008.

## References

1 J. O. M. Bockris, The Origin of Ideas on a Hydrogen Economy and Its Solution to the Decay of the Environment, *Int. J. Hydrogen Energy*, 2002, **27**, 731–740.
2 S. Anantharaj, S. R. Ede, K. Sakthikumar, K. Karthick, S. Mishra and S. Kundu, Recent Trends and Perspectives in Electrochemical Water Splitting with an Emphasis on Sulfide, Selenide, and Phosphide Catalysts of Fe, Co, and Ni: A Review, *ACS Catal.*, 2016, **6**, 8069–8097.
3 Y. Jiao, Y. Zheng, M. Jaroniec and S. Z. Qiao, Design of Electrocatalysts for Oxygen- and Hydrogen-Involving Energy Conversion Reactions, *Chem. Soc. Rev.*, 2015, **44**, 2060–2086.
4 A. Karmakar, K. Karthick, S. S. Sankar, S. Kumaravel, R. Madhu and S. Kundu, A Vast Exploration of Improvising Synthetic Strategies for Enhancing the OER Kinetics of LDH Structures: A Review, *J. Mater. Chem. A*, 2021, **9**, 1314–1352.
5 K. Karthick, S. Anantharaj, S. R. Ede and S. Kundu, Nanosheets of Nickel Iron Hydroxy Carbonate Hydrate with Pronounced OER Activity under Alkaline and Near-Neutral Conditions, *Inorg. Chem.*, 2019, **58**, 1895–1904.
6 Q. Yao, B. Huang, N. Zhang, M. Sun, Q. Shao and X. Huang, Channel-Rich RuCu Nanosheets for PH-Universal Overall Water Splitting Electrocatalysis, *Angew. Chem., Int. Ed.*, 2019, **58**, 13983–13988.
7 R. D. Cortright, R. R. Davda and J. A. Dumesic, Hydrogen from Catalytic Reforming of Biomass-Derived Hydrocarbons in Liquid Water, *Nature*, 2002, **418**, 964–967.
8 J. Su, Y. Yang, G. Xia, J. Chen, P. Jiang and Q. Chen, Ruthenium-Cobalt Nanoalloys Encapsulated in Nitrogen-Doped Graphene as Active Electrocatalysts for Producing Hydrogen in Alkaline Media, *Nat. Commun.*, 2017, **8**, 1–10.

 

9 Y. Wang, D. Yan, S. El Hankari, Y. Zou and S. Wang, Recent Progress on Layered Double Hydroxides and Their Derivatives for Electrocatalytic Water Splitting, *Adv. Sci.*, 2018, **5**, 1800064.
10 S. Kumaravel, K. Karthick, S. S. Sankar, A. Karmakar, R. Madhu, K. Bera and S. Kundu, Current Progressions in Transition Metal Based Hydroxides as Bi-Functional Catalysts towards Electrocatalytic Total Water Splitting, *Sustainable Energy Fuels*, 2021, **5**, 6215–6268.
11 S. Sanati, A. Morsali and H. García, First-Row Transition Metal-Based Materials Derived from Bimetallic Metal–Organic Frameworks as Highly Efficient Electrocatalysts for Electrochemical Water Splitting, *Energy Environ. Sci.*, 2022, **15**, 3119–3151.
12 Y. Pan, R. Abazari, Y. Wu, J. Gao and Q. Zhang, Advances in metal–organic frameworks and their derivatives for diverse electrocatalytic applications, *Electrochem. Commun.*, 2021, **126**, 107024.
13 J. Chen, R. Abazari, K. A. Adegoke, N. W. Maxakato, O. S. Bello, M. Tahir, S. Tasleem, S. Sanati, A. M. Kirillov and Y. Zhou, Metal–Organic Frameworks and Derived Materials as Photocatalysts for Water Splitting and Carbon Dioxide Reduction, *Coord. Chem. Rev.*, 2022, **469**, 214664.
14 S. S. Sankar, K. Karthick, K. Sangeetha, A. Karmakar, R. Madhu and S. Kundu, Current Perspectives on 3D ZIFs Incorporated with 1D Carbon Matrices as Fibers via Electrospinning Processes towards Electrocatalytic Water Splitting: A Review, *J. Mater. Chem. A*, 2021, **9**, 11961–12002.
15 Y. Zhang and L. Qi, MOF-Derived Nanoarrays as Advanced Electrocatalysts for Water Splitting, *Nanoscale*, 2022, **14**, 12196–12218.
16 R. Goswami, A. Karmakar, S. Rajput, M. Singh, S. Kundu and S. Neogi, Deciphering the Role of Functional Synergy in a Catalytic Molecular Assembler: A Proof-of-Concept to Boosted Catalysis via Retrosynthetic Linker Scissoring, *Mater. Chem. Front.*, 2023, **7**, 881–896.
17 A. Mahmood, W. Guo, H. Tabassum and R. Zou, Metal–Organic Framework-Based Nanomaterials for Electrocatalysis, *Adv. Energy Mater.*, 2016, **6**, 1600423.
18 Y. Li, M. Lu, Y. Wu, Q. Ji, H. Xu, J. Gao, G. Qian and Q. Zhang, Morphology Regulation of Metal–Organic Framework-Derived Nanostructures for Efficient Oxygen Evolution Electrocatalysis, *J. Mater. Chem. A*, 2020, **8**, 18215–18219.
19 Y. Wu, Y. Li, J. Gao and Q. Zhang, Recent advances in vacancy engineering of metal–organic frameworks and their derivatives for electrocatalysis, *SusMat*, 2021, **1**, 66–87.
20 H. Li, M. Eddaoudi, M. O'Keeffe and O. M. Yaghi, Design and synthesis of an exceptionally stable and highly porous metal–organic framework, *Nature*, 1999, **402**, 276–279.
21 L. Chai, J. Pan, Y. Hu, J. Qian and M. Hong, Rational Design and Growth of MOF-on-MOF Heterostructures, *Small*, 2021, **17**, 1–31.
22 S. Anantharaj, S. R. Ede, K. Karthick, S. Sam Sankar, K. Sangeetha, P. E. Karthik and S. Kundu, Precision and Correctness in the Evaluation of Electrocatalytic Water Splitting: Revisiting Activity Parameters with a Critical Assessment, *Energy Environ. Sci.*, 2018, **11**, 744–771.
23 Y. Yao, Z. Zhang and L. Jiao, Development Strategies in Transition Metal Borides for Electrochemical Water Splitting, *Energy Environ. Mater.*, 2022, **5**, 470–485.
24 S. Li, Y. Gao, N. Li, L. Ge, X. Bu and P. Feng, Transition Metal-Based Bimetallic MOFs and MOF-Derived Catalysts for Electrochemical Oxygen Evolution Reaction, *Energy Environ. Sci.*, 2021, **14**, 1897–1927.
25 K. Zhang and R. Zou, Advanced Transition Metal-Based OER Electrocatalysts: Current Status, Opportunities, and Challenges, *Small*, 2021, **17**, 1–40.
26 Z. P. Wu, X. F. Lu, S. Q. Zang and X. W. Lou, Non-Noble-Metal-Based Electrocatalysts toward the Oxygen Evolution Reaction, *Adv. Funct. Mater.*, 2020, **30**, 1–20.
27 M. Rubio-Martinez, C. Avci-Camur, A. W. Thornton, I. Imaz, D. Maspoch and M. R. Hill, New Synthetic Routes towards MOF Production at Scale, *Chem. Soc. Rev.*, 2017, **46**, 3453–3480.
28 A. Rehman, S. A. Tirmizi, A. Badshah, H. M. Ammad, M. Jawad, S. M. Abbas, U. A. Rana and S. U. D. Khan, Synthesis of Highly Stable MOF-5@MWCNTs Nanocomposite with Improved Hydrophobic Properties, *Arab. J. Chem.*, 2018, **11**, 26–33.
29 P. Li, F. F. Cheng, W. W. Xiong and Q. Zhang, New Synthetic Strategies to Prepare Metal–Organic Frameworks, *Inorg. Chem. Front.*, 2018, **5**, 2693–2708.
30 C. P. Raptopoulou, Metal–Organic Frameworks: Synthetic Methods and Potential Applications, *Materials*, 2021, **14**, 1–32.
31 R. Goswami, K. Karthick, S. Das, S. Rajput, N. Seal, B. Pathak, S. Kundu and S. Neogi, Brønsted Acid-Functionalized Ionic Co(II) Framework: A Tailored Vessel for Electrocatalytic Oxygen Evolution and Size-Exclusive Optical Speciation of Biothiols, *ACS Appl. Mater. Interfaces*, 2022, **14**, 29773–29787.
32 V. R. Remya and M. Kurian, Synthesis and Catalytic Applications of Metal–Organic Frameworks: A Review on Recent Literature, *Int. Nano Lett.*, 2019, **9**, 17–29.
33 C. Dey, T. Kundu, B. P. Biswal, A. Mallick and R. Banerjee, Crystalline Metal–Organic Frameworks (MOFs): Synthesis, Structure and Function, *Acta Crystallogr., Sect. B: Struct. Sci., Cryst. Eng. Mater.*, 2014, **70**, 3–10.
34 G. Li, S. Zhao, Y. Zhang and Z. Tang, Metal–Organic Frameworks Encapsulating Active Nanoparticles as Emerging Composites for Catalysis: Recent Progress and Perspectives, *Adv. Mater.*, 2018, **30**, 1–43.
35 J. H. Cavka, S. Jakobsen, U. Olsbye, N. Guillou, C. Lamberti, S. Bordiga and K. P. Lillerud, A New Zirconium Inorganic Building Brick Forming Metal Organic Frameworks with Exceptional Stability, *J. Am. Chem. Soc.*, 2008, **130**, 13850–13851.
36 M. Zhao, K. Yuan, Y. Wang, G. Li, J. Guo, L. Gu, W. Hu, H. Zhao and Z. Tang, Metal–Organic Frameworks as Selectivity Regulators for Hydrogenation Reactions, *Nature*, 2016, **539**, 76–80.

37 A. Aijaz, A. Karkamkar, Y. J. Choi, N. Tsumori, E. Rönnebro, T. Autrey, H. Shioyama and Q. Xu, Immobilizing Highly Catalytically Active Pt Nanoparticles inside the Pores of Metal–Organic Framework: A Double Solvents Approach, *J. Am. Chem. Soc.*, 2012, **134**, 13926–13929.
38 K. M. L. Taylor-Pashow, J. Della Rocca, Z. Xie, S. Tran and W. Lin, Postsynthetic Modifications of Iron-Carboxylate Nanoscale Metal–Organic Frameworks for Imaging and Drug Delivery, *J. Am. Chem. Soc.*, 2009, **131**, 14261–14263.
39 B. Rungtaweevoranit, J. Baek, J. R. Araujo, B. S. Archanjo, K. M. Choi, O. M. Yaghi and G. A. Somorjai, Copper Nanocrystals Encapsulated in Zr-Based Metal–Organic Frameworks for Highly Selective $CO_2$ Hydrogenation to Methanol, *Nano Lett.*, 2016, **16**, 7645–7649.
40 Y. Peng and W. Yang, Metal–Organic Framework Nanosheets: A Class of Glamorous Low-Dimensional Materials with Distinct Structural and Chemical Natures, *Sci. China: Chem.*, 2019, **62**, 1561–1575.
41 G. Hai, X. Jia, K. Zhang, X. Liu, Z. Wu and G. Wang, High-Performance Oxygen Evolution Catalyst Using Two-Dimensional Ultrathin Metal–Organic Frameworks Nanosheets, *Nano Energy*, 2018, **44**, 345–352.
42 W. Cheng, X. Zhao, H. Su, F. Tang, W. Che, H. Zhang and Q. Liu, Lattice-Strained Metal–Organic-Framework Arrays for Bifunctional Oxygen Electrocatalysis, *Nat. Energy*, 2019, **4**, 115–122.
43 U. Khan, A. Nairan, J. Gao and Q. Zhang, Current Progress in 2D Metal–Organic Frameworks for Electrocatalysi, *Small Struct.*, 2022, **2200109**, 2200109.
44 J. Huang, Y. Li, R. Huang, C. He, L. Gong, Q. Hu, L. Wang, Y. Xu, X. Tian, S. Liu, Z. Ye, F. Wang, D. Zhou, W. Zhang and J. Zhang, Electrochemical Exfoliation of Pillared-Layer Metal–Organic Framework to Boost the Oxygen Evolution Reaction, *Angew. Chem.*, 2018, **130**, 4722–4726.
45 T. Guo, L. Chen, Y. Li and K. Shen, Controllable Synthesis of Ultrathin Defect-Rich LDH Nanoarrays Coupled with MOF-Derived Co-NC Microarrays for Efficient Overall Water Splitting, *Small*, 2021, **18**, 2107739.
46 Y. Xu, B. Li, S. Zheng, P. Wu, J. Zhan, H. Xue, Q. Xu and H. Pang, Ultrathin Two-Dimensional Cobalt–Organic Framework Nanosheets for High-Performance Electrocatalytic Oxygen Evolution, *J. Mater. Chem. A*, 2018, **6**, 22070–22076.
47 G. Zhan and H. C. Zeng, Synthesis and Functionalization of Oriented Metal–Organic-Framework Nanosheets: Toward a Series of 2D Catalysts, *Adv. Funct. Mater.*, 2016, **26**, 3268–3281.
48 M. Cai, Q. Liu, Z. Xue, Y. Li, Y. Fan, A. Huang, M. R. Li, M. Croft, T. A. Tyson, Z. Ke and G. Li, Constructing 2D MOFs from 2D LDHs: A Highly Efficient and Durable Electrocatalyst for Water Oxidation, *J. Mater. Chem. A*, 2020, **8**, 190–195.
49 X. Mu, H. Yuan, H. Jing, F. Xia, J. Wu, X. Gu, C. Chen, J. Bao, S. Liu and S. Mu, Superior Electrochemical Water Oxidation in Vacancy Defect-Rich 1.5 Nm Ultrathin Trimetal–Organic Framework Nanosheets, *Appl. Catal., B*, 2021, **296**, 120095.
50 L. Zhuang, L. Ge, H. Liu, Z. Jiang, Y. Jia, Z. Li, D. Yang, R. K. Hocking, M. Li, L. Zhang, X. Wang, X. Yao and Z. Zhu, A Surfactant-Free and Scalable General Strategy for Synthesizing Ultrathin Two-Dimensional Metal–Organic Framework Nanosheets for the Oxygen Evolution Reaction, *Angew. Chem., Int. Ed.*, 2019, **58**, 13565–13572.
51 T. Wen, Y. Zheng, J. Zhang, K. Davey and S. Z. Qiao, Co(II) Boron Imidazolate Framework with Rigid Auxiliary Linkers for Stable Electrocatalytic Oxygen Evolution Reaction, *Adv. Sci.*, 2019, **6**, 1–5.
52 Y. Li, Y. Wu, T. Li, M. Lu, Y. Chen, Y. Cui, J. Gao and G. Qian, Tuning the Electronic Structure of a Metal–Organic Framework for an Efficient Oxygen Evolution Reaction by Introducing Minor Atomically Dispersed Ruthenium, *Carbon Energy*, 2022, 1–11, DOI: **10.1002/cey2.265**.
53 Z. Y. Zhao, X. Sun, H. Gu, Z. Niu, P. Braunstein and J. P. Lang, Engineering the Electronic Structures of Metal–Organic Framework Nanosheets via Synergistic Doping of Metal Ions and Counteranions for Efficient Water Oxidation, *ACS Appl. Mater. Interfaces*, 2022, **14**, 15133–15140.
54 J. Zhou, Z. Han, X. Wang, H. Gai, Z. Chen, T. Guo, X. Hou, L. Xu, X. Hu, M. Huang, S. V. Levchenko and H. Jiang, Discovery of Quantitative Electronic Structure-OER Activity Relationship in Metal–Organic Framework Electrocatalysts Using an Integrated Theoretical-Experimental Approach, *Adv. Funct. Mater.*, 2021, **31**, 1–13.
55 R. Zhu, J. Ding, Y. Xu, J. Yang, Q. Xu and H. Pang, π-Conjugated Molecule Boosts Metal–Organic Frameworks as Efficient Oxygen Evolution Reaction Catalysts, *Small*, 2018, **14**, 1–6.
56 W. C. Hu, Y. Shi, Y. Zhou, C. Weng, M. R. Younis, J. Pang, C. Wang and X. H. Xia, Plasmonic Hot Charge Carriers Activated Ni Centres of Metal–Organic Frameworks for the Oxygen Evolution Reaction, *J. Mater. Chem. A*, 2019, **7**, 10601–10609.
57 Y. Guo, T. Wang, J. Chen, J. Zheng, X. Li and K. (Ken) Ostrikov, Air Plasma Activation of Catalytic Sites in a Metal-Cyanide Framework for Efficient Oxygen Evolution Reaction, *Adv. Energy Mater.*, 2018, **8**, 1–8.
58 S. Kandambeth, V. S. Kale, D. Fan, J. A. Bau, P. M. Bhatt, S. Zhou, A. Shkurenko,. Rueping, G. Maurin, O. Shekhah and M. Eddaoudi, Unveiling Chemically Robust Bimetallic Squarate-Based Metal–Organic Frameworks for Electrocatalytic Oxygen Evolution Reaction, *Adv. Energy Mater.*, 2023, **13**, 2202964.
59 X. F. Lu, P. Q. Liao, J. W. Wang, J. X. Wu, X. W. Chen, C. T. He, J. P. Zhang, G. R. Li and X. M. Chen, An Alkaline-Stable, Metal Hydroxide Mimicking Metal–Organic Framework for Efficient Electrocatalytic Oxygen Evolution, *J. Am. Chem. Soc.*, 2016, **138**, 8336–8339.
60 Z. Zou, T. Wang, X. Zhao, W. J. Jiang, H. Pan, D. Gao and C. Xu, Expediting In-Situ Electrochemical Activation of Two-Dimensional Metal–Organic Frameworks for Enhanced OER Intrinsic Activity by Iron Incorporation, *ACS Catal.*, 2019, **9**, 7356–7364.

 

61 R. Madhu, S. S. Sankar, K. Karthick, A. Karmakar, S. Kumaravel and S. Kundu, Electrospun Cobalt-Incorporated MOF-5 Microfibers as a Promising Electrocatalyst for OER in Alkaline Media, *Inorg. Chem.*, 2021, **60**, 9899–9911.
62 T. Y. Ma, S. Dai, M. Jaroniec and S. Z. Qiao, Metal–Organic Framework Derived Hybrid $Co_3O_4$-Carbon Porous Nanowire Arrays as Reversible Oxygen Evolution Electrodes, *J. Am. Chem. Soc.*, 2014, **136**, 13925–13931.
63 L. Pei, J. Zhong, T. Li, W. Bai, S. Wu, Y. Yuan, Y. Chen, Z. Yu, S. Yan and Z. Zou, CoS2@N-Doped Carbon Core–Shell Nanorod Array Grown on Ni Foam for Enhanced Electrocatalytic Water Oxidation, *J. Mater. Chem. A*, 2020, **8**, 6795–6803.
64 A. Goswami, D. Ghosh, D. Pradhan and K. Biradha, In Situ Grown Mn(II) MOF upon Nickel Foam Acts as a Robust Self-Supporting Bifunctional Electrode for Overall Water Splitting: A Bimetallic Synergistic Collaboration Strategy, *ACS Appl. Mater. Interfaces*, 2022, **14**, 29722–29734.
65 W. Xie, Y. Song, S. Li, J. Li, Y. Yang, W. Liu, M. Shao and M. Wei, Single-Atomic-Co Electrocatalysts with Self-Supported Architecture toward Oxygen-Involved Reaction, *Adv. Funct. Mater.*, 2019, **29**, 1–8.
66 J. Rong, F. Qiu, T. Zhang, Y. Fang, J. Xu and Y. Zhu, Self-Directed Hierarchical $Cu_3(PO_4)_2$/Cu-BDC Nanosheets Array Based on Copper Foam as an Efficient and Durable Electrocatalyst for Overall Water Splitting, *Electrochim. Acta*, 2019, **313**, 179–188.
67 G. Genesio, J. Maynadié, M. Carboni and D. Meyer, Recent Status on MOF Thin Films on Transparent Conductive Oxides Substrates (ITO or FTO), *New J. Chem.*, 2018, **42**, 2351–2363.
68 R. Madhu, S. S. Sankar, K. Karthick, A. Karmakar, S. Kumaravel and S. Kundu, Electrospun Cobalt-Incorporated MOF-5 Microfibers as a Promising Electrocatalyst for OER in Alkaline Media, *Inorg. Chem.*, 2021, **60**, 9899–9911.
69 C. Wang, H. Shang, J. Li, Y. Wang, H. Xu, C. Wang, J. Guo and Y. Du, Ultralow Ru Doping Induced Interface Engineering in MOF Derived Ruthenium-Cobalt Oxide Hollow Nanobox for Efficient Water Oxidation Electrocatalysis, *Chem. Eng. J.*, 2021, **420**, 129805.
70 Y. Wang, C. Wang, H. Shang, M. Yuan, Z. Wu, J. Li and Y. Du, Self-Driven Ru-Modified NiFe MOF Nanosheet as Multifunctional Electrocatalyst for Boosting Water and Urea Electrolysis, *J. Colloid Interface Sci.*, 2022, **605**, 779–789.
71 Y. Fu, W. Wang, J. Wang, X. Li, R. Shi, O. Peng, B. N. Chandrashekar, K. Liu, A. Amini and C. Cheng, *J. Mater. Chem. A*, 2019, **7**, 17299–17305.
72 Y. Fu, W. Wang, J. Wang, X. Li, R. Shi, O. Peng, B. N. Chandrashekar, K. Liu, A. Amini and C. Cheng, MOFs-Derived ZnCo–Fe Core–Shell Nanocages with Remarkable Oxygen Evolution Reaction Performance, *J. Mater. Chem. A*, 2019, **7**, 17299–17305.
73 X. Wang, H. Xiao, A. Li, Z. Li, S. Liu, Q. Zhang, Y. Gong, L. Zheng, Y. Zhu, C. Chen, D. Wang, Q. Peng, L. Gu, X. Han, J. Li and Y. Li, Constructing NiCo/$Fe_3O_4$ Heteroparticles within MOF-74 for Efficient Oxygen Evolution Reactions, *J. Am. Chem. Soc.*, 2018, **140**, 15336–15341.
74 C. Wang and L. Qi, Heterostructured Inter-Doped Ruthenium–Cobalt Oxide Hollow Nanosheet Arrays for Highly Efficient Overall Water Splitting, *Angew. Chem., Int. Ed.*, 2020, **59**, 17219–17224.
75 R. Madhu, A. Karmakar, S. Kumaravel, S. S. Sankar, K. Bera, S. Nagappan, H. N. Dhandapani and S. Kundu, Revealing the PH-Universal Electrocatalytic Activity of Co-Doped $RuO_2$ toward the Water Oxidation Reaction, *ACS Appl. Mater. Interfaces*, 2022, **14**, 1077–1091.
76 J. Du, F. Li and L. Sun, Metal–Organic Frameworks and Their Derivatives as Electrocatalysts for the Oxygen Evolution Reaction, *Chem. Soc. Rev.*, 2021, **50**, 2663–2695.
77 T. I. Singh, G. Rajeshkhanna, U. N. Pan, T. Kshetri, H. Lin, N. H. Kim and J. H. Lee, Alkaline Water Splitting Enhancement by MOF-Derived Fe–Co–Oxide/Co@NC-MNS Heterostructure: Boosting OER and HER through Defect Engineering and In Situ Oxidation, *Small*, 2021, **17**, 1–14.
78 H. Sun, Y. Lian, C. Yang, L. Xiong, P. Qi, Q. Mu, X. Zhao, J. Guo, Z. Deng and Y. Peng, A Hierarchical Nickel-Carbon Structure Templated by Metal–Organic Frameworks for Efficient Overall Water Splitting, *Energy Environ. Sci.*, 2018, **11**, 2363–2371.
79 Q. Yuan, Y. Yu, Y. Gong and X. Bi, Three-Dimensional N-Doped Carbon Nanotube Frameworks on Ni Foam Derived from a Metal–Organic Framework as a Bifunctional Electrocatalyst for Overall Water Splitting, *ACS Appl. Mater. Interfaces*, 2020, **12**, 3592–3602.
80 H. Xu, Z. X. Shi, Y. X. Tong and G. R. Li, A Porous Microrod Arrays Constructed by Carbon-Confined NiCo@$NiCoO_2$ Core@Shell Nanoparticles as Efficient Electrocatalysts for Oxygen Evolution, *Adv. Mater.*, 2018, **30**, 1–8.
81 L. Yan, Y. Xu, P. Chen, S. Zhang, H. Jiang, L. Yang, Y. Wang, L. Zhang, J. Shen, X. Zhao and L. Wang, A Freestanding 3D Heterostructure Film Stitched by MOF-Derived Carbon Nanotube Microsphere Superstructure and Reduced Graphene Oxide Sheets: A Superior Multifunctional Electrode for Overall Water Splitting and Zn–Air Batteries, *Adv. Mater.*, 2020, **32**, 1–11.
82 Z. Chen, R. Wu, M. Liu, Y. Liu, S. Xu, Y. Ha, Y. Guo, X. Yu, D. Sun and F. Fang, Tunable Electronic Coupling of Cobalt Sulfide/Carbon Composites for Optimizing Oxygen Evolution Reaction Activity, *J. Mater. Chem. A*, 2018, **6**, 10304–10312.
83 C. Walter, P. W. Menezes, S. Orthmann, J. Schuch, P. Connor, B. Kaiser, M. Lerch and M. Driess, A Molecular Approach to Manganese Nitride Acting as a High Performance Electrocatalyst in the Oxygen Evolution Reaction, *Angew. Chem., Int. Ed.*, 2018, **57**, 698–702.
84 C. Gu, S. Hu, X. Zheng, M. R. Gao, Y. R. Zheng, L. Shi, Q. Gao, X. Zheng, W. Chu, H. Bin Yao, J. Zhu and S. H. Yu, Synthesis of Sub-2 Nm Iron-Doped $NiSe_2$ Nanowires and Their Surface-Confined Oxidation for Oxygen Evolution Catalysis, *Angew. Chem., Int. Ed.*, 2018, **57**, 4020–4024.

85 Z. H. Xue, H. Su, Q. Y. Yu, B. Zhang, H. H. Wang, X. H. Li and J. S. Chen, anus Co/CoP Nanoparticles as Efficient Mott–Schottky Electrocatalysts for Overall Water Splitting in Wide PH Range, *Adv. Energy Mater.*, 2017, **7**, 1–7.

86 J. Joo, T. Kim, J. Lee, S. Il Choi and K. Lee, Morphology-Controlled Metal Sulfides and Phosphides for Electrochemical Water Splitting, *Adv. Mater.*, 2019, **31**, 1–23.

87 J. Masud, P. C. Ioannou, N. Levesanos, P. Kyritsis and M. Nath, A Molecular Ni-Complex Containing Tetrahedral Nickel Selenide Core as Highly Efficient Electrocatalyst for Water Oxidation, *ChemSusChem*, 2016, **9**, 3128–3132.

88 J. G. Li, H. Sun, L. Lv, Z. Li, X. Ao, C. Xu, Y. Li and C. Wang, Metal–Organic Framework-Derived Hierarchical (Co,Ni)$Se_2$ @NiFe LDH Hollow Nanocages for Enhanced Oxygen Evolution, *ACS Appl. Mater. Interfaces*, 2019, **11**, 8106–8114.

89 G. Fang, Q. Wang, J. Zhou, Y. Lei, Z. Chen, Z. Wang, A. Pan and S. Liang, Metal Organic Framework-Templated Synthesis of Bimetallic Selenides with Rich Phase Boundaries for Sodium-Ion Storage and Oxygen Evolution Reaction, *ACS Nano*, 2019, **13**, 5635–5645.

90 W. Song, X. Teng, Y. Liu, J. Wang, Y. Niu, X. He, C. Zhang and Z. Chen, Rational Construction of Self-Supported Triangle-like MOF-Derived Hollow (Ni,Co)$Se_2$ Arrays for Electrocatalysis and Supercapacitors, *Nanoscale*, 2019, **11**, 6401–6409.

91 Y. Guo, C. Zhang, J. Zhang, K. Dastafkan, K. Wang, C. Zhao and Z. Shi, Metal–Organic Framework-Derived Bimetallic NiFe Selenide Electrocatalysts with Multiple Phases for Efficient Oxygen Evolution Reaction, *ACS Sustainable Chem. Eng.*, 2021, **9**, 2047–2056.

92 M. I. da Silva, Í. R. Machado, H. E. Toma, K. Araki, L. Angnes and J. M. Gonçalves, Recent Progress in Water-Splitting and Supercapacitor Electrode Materials Based on MOF-Derived Sulfides, *J. Mater. Chem. A*, 2022, **10**, 430–474.

93 P. He, Y. Xie, Y. Dou, J. Zhou, A. Zhou, X. Wei and J. R. Li, Partial Sulfurization of a 2D MOF Array for Highly Efficient Oxygen Evolution Reaction, *ACS Appl. Mater. Interfaces*, 2019, **11**, 41595–41601.

94 M. Zhao, W. Li, J. Li, W. Hu and C. M. Li, Strong Electronic Interaction Enhanced Electrocatalysis of Metal Sulfide Clusters Embedded Metal–Organic Framework Ultrathin Nanosheets toward Highly Efficient Overall Water Splitting, *Adv. Sci.*, 2020, **7**(20), 1–10, DOI: **10.1002/advs.202001965**.

95 Y. Lin, G. Chen, H. Wan, F. Chen, X. Liu and R. Ma, Free-Standing Nitrogen-Doped Ni–$Ni_3S_2$ @Carbon Nanoplates Derived from Metal–Organic Frameworks for Enhanced Oxygen Evolution Reaction, *Small*, 2019, **15**, 1–11.

96 Y. J. Lee and S. K. Park, Metal–Organic Framework-Derived Hollow $CoS_x$ Nanoarray Coupled with NiFe Layered Double Hydroxides as Efficient Bifunctional Electrocatalyst for Overall Water Splitting, *Small*, 2022, **18**, 1–10.

97 X. Zhang, J. Li, Y. Yang, S. Zhang, H. Zhu, X. Zhu, H. Xing, Y. Zhang, B. Huang, S. Guo and E. Wang, Interface Nanowire for Enhancing Water Oxidation Catalysis at High Current Density, *Adv. Mater.*, 2018, **30**, 1–8.

98 D. Chen, R. Lu, Z. Pu, J. Zhu, H. W. Li, F. Liu, S. Hu, X. Luo, J. Wu, Y. Zhao and S. Mu, Ru-Doped 3D Flower-like Bimetallic Phosphide with a Climbing Effect on Overall Water Splitting, *Appl. Catal., B*, 2020, **279**, 119396.

99 D. Yang, Z. Su, Y. Chen, K. Srinivas, J. Gao, W. Zhang, Z. Wang and H. Lin, Electronic Modulation of Hierarchical Spongy Nanosheets toward Efficient and Stable Water Electrolysis, *Small*, 2021, **17**, 1–10.

100 R. B. Ghising, U. N. Pan, D. R. Paudel, M. R. Kandel, N. H. Kim and J. H. Lee, A Hybrid Trimetallic–Organic Framework-Derived N,C Co-Doped Ni–Fe–Mn–P Ultrathin Nanosheet Electrocatalyst for Proficient Overall Water-Splitting, *J. Mater. Chem. A*, 2022, **10**, 16457–16467.

101 B. Zhang, C. Xiao, S. Xie, J. Liang, X. Chen and Y. Tang, Iron–Nickel Nitride Nanostructures in Situ Grown on Surface-Redox-Etching Nickel Foam: Efficient and Ultrasustainable Electrocatalysts for Overall Water Splitting, *Chem. Mater.*, 2016, **28**, 6934–6941.

102 X. Shi, A. Wu, H. Yan, L. Zhang, C. Tian, L. Wang and H. Fu, A ''MOFs plus MOFs'' Strategy toward Co-$Mo_2N$ Tubes for Efficient Electrocatalytic Overall Water Splitting, *J. Mater. Chem. A*, 2018, **6**, 20100–20109.

103 B. K. Kang, S. Y. Im, J. Lee, S. H. Kwag, S. Bin Kwon, S. N. Tiruneh, M. J. Kim, J. H. Kim, W. S. Yang, B. Lim and D. H. Yoon, *Nano Res.*, 2019, **12**, 1605–1611.

104 Y. Wang, J. Ma, J. Wang, S. Chen, H. Wang and J. Zhang, Interfacial Scaffolding Preparation of Hierarchical PBA-Based Derivative Electrocatalysts for Efficient Water Splitting, *Adv. Energy Mater.*, 2019, **9**, 1–11.

105 M. Liu, W. Zheng, S. Ran, S. T. Boles and L. Y. S. Lee, Overall Water-Splitting Electrocatalysts Based on 2D CoNi–Metal–Organic Frameworks and Its Derivative, *Adv. Mater. Interfaces*, 2018, **5**, 1–8.

106 Y. Li, L. X. Song, W. P. Wang, Y. Teng, J. Xia and N. N. Liu, Morphological Transformation, Photocatalytic Properties, and Electrocatalytic OER Performance of Fe-MOF Nanopolyhedra, *J. Phys. Chem. C*, 2021, **125**, 27207–27220.

107 J. Cheng, X. Shen, H. Chen, H. Zhou, P. Chen, Z. Ji, Y. Xue, H. Zhou and G. Zhu, Morphology-Dependent Electrocatalytic Performance of a Two-Dimensional Nickel–Iron MOF for Oxygen Evolution Reaction, *Inorg. Chem.*, 2022, **61**, 7095–7102.

 